Multiple Autonomous Underwater Vehicle Cooperative Localization in Anchor-Free Environments

Yichen Li, *Student Member, IEEE*, Yiyin Wang, *Member, IEEE*, Wenbin Yu, *Member, IEEE*, and Xinping Guan, *Fellow, IEEE*

***Abstract*—The localization of autonomous underwater vehicles (AUVs) in anchor-free environments has always been a difficult problem due to the lack of global positioning systems and absolute references. In general, AUVs localize themselves by dead reckoning (DR), whereas the localization error grows without bound. To alleviate the growth of the localization errors, we propose intermittent belief propagation based dead reckoning (IBPDR) as a cooperative localization (CL) framework. In IBPDR, AUVs use DR to localize themselves and periodically correct DR's deviation with CL methods. The intermittent feature of IBPDR reduces communication costs among AUVs by decreasing the frequency of CL. In the IBPDR framework, we design a particle-based underwater-adaptive belief propagation (UABP) algorithm for CL. The UABP algorithm is naturally distributed and viable in nonlinear and non-Gaussian situations. Thus, it is suitable for CL issues. Furthermore, the UABP algorithm is robust to the accumulated inertial measurement errors and reduces communication costs among AUVs. Moreover, we propose a particle-based current-aided filter to further improve the localization accuracy by comparing AUVs' ambient current observations with the available current maps. Simulation results validate the proposed algorithms by comparisons with alternative approaches in localization accuracy, communication costs, and robustness to abnormal cases, such as packet loss, ranging bias, and outliers.**

***Index Terms*—Anchor-free, autonomous underwater vehicles (AUVs), cooperative localization (CL), intermittent.**

I. Introduction

AUTONOMOUS underwater vehicle (AUV) localization has always been a difficult task [1], [2]. It is due to the unavailability of global positioning system (GPS) signals, the harsh channel conditions for underwater acoustics [3], the complex marine environments, etc. In general, AUVs localize themselves by using inertial measurements (heading angles and speeds) from inertial measurement units (IMUs) with dead reckoning (DR). However, due to the accumulated errors in the inertial measurements, the localization error of DR grows without bound [4]. Hence, using DR alone leads to a short-time reliability. To correct these errors, AUVs usually periodically resurface to calibrate their positions by GPS. The problem is that resurfacing consumes considerable amount of energy and is impossible in some circumstances, such as navigating in ice-covered polar regions. With the development of underwater acoustic communications and localization techniques, AUV localization can be solved by interaction with anchors (devices with known positions). Typical examples are the baseline systems [5]. Nevertheless, under the current situations, anchors are only deployed in very limited regions, and the expenses of anchor deployment and maintenance are considerably high [6]. Thus, anchor-free environments widely exist, and corresponding AUV localization methods are in urgent demand. When AUVs navigate in anchor-free environments, without any assistance of anchors, cooperative localization (CL) among AUVs is a viable option to improve the localization accuracy. It has been proved that CL can provide higher localization accuracy compared with noncooperative localization [7], [8]. Moreover, cooperations among AUVs can also result in higher operational abilities and become more and more popular in applications [9], [10]. In this article, CL methods are used to improve the localization when AUVs are navigating in anchor-free environments.

In previous works, many CL methods for wireless sensor networks (WSNs) have been designed [11]–[15]. Extended Kalman filter is a popular one and widely applied in CL problems [16]–[18]. Another well-known algorithm, belief propagation (BP) [19], is also commonly used in CL. BP is a naturally distributed message-passing algorithm. It is able to compute the marginal posterior distributions of individual devices' positions in a distributed fashion. Furthermore, the complexity of BP grows only linearly to the network size. Thus, it has good scalability. Many applications of BP in mobile devices CL have been developed in [20]–[23]. However, these methods are not suitable for AUV localization. In reality, AUVs use the inertial measurements to predict their positions. The prediction can be severely affected by the accumulated errors in the inertial measurements. In [20]–[23], the applied position prediction models are usually with

Manuscript received January 14, 2019; revised July 27, 2019; accepted August 9, 2019. Date of publication September 6, 2019; date of current version October 11, 2019. This work was supported in part by the National Nature Science Foundation of China under Grant 61633017, Grant 61773264, and Grant 61803261, in part by the United Fund of Department of Equipment Development and Ministry of Education of China under Grant 6141A02033317, and in part by Shanghai Natural Science Foundation of China under Grant 18ZR1421100. The preliminary version of this work was presented at the Underwater Communications and Networking conference, Lerici, Italy, August 28–30, 2018. *(Corresponding author: Yiyin Wang.)*

Guest Editor: J. Alves.

The authors are with the Department of Automation, Key Laboratory of System Control and Information Processing (Ministry of Education of China), and State Key Laboratory of Ocean Engineering, Shanghai Jiao Tong University, Shanghai 200240, China (e-mail: liyichensjtu@sjtu.edu.cn; yiyinwang@sjtu.edu.cn; yuwenbin@sjtu.edu.cn; xpguan@sjtu.edu.cn).

Digital Object Identifier 10.1109/JOE.2019.2935516

constant velocities, and do not consider the accumulated errors in the prediction. Another challenge in CL is the wide existences of the nonlinear non-Gaussian cases, which leads to the design of BP variations [24]–[27]. Statistical linear regression and unscented transform are used in [24] and [25], respectively, to deal with the nonlinearities. Different types of non-Gaussian models are applied in [26] and [27]. Particle-based BP [28], [29] is another important variant of BP. It is able to deal with both nonlinear and non-Gaussian cases. Moreover, it can provide position estimates as well as the corresponding uncertainties. In CL, reducing the communication costs is important, especially in particle-based methods. The transmission volume of hundreds of (maybe more) particles is much larger than that of several parameters in parametric methods. In underwater applications, due to energy limitations of underwater devices, reducing the communication costs becomes more necessary. In [28] and [30], Gaussian mixture model is used to approximate the transmitted particles. In [31], a position vector and a covariance matrix are used to represent the position estimate when the estimation results need to be transmitted.

So far, most previous works on multi-AUV CL involve anchors, which could be well-equipped leader vehicles [32]–[34], communication and navigation aids (CNAs) [35], [36], and other kinds of devices with known positions. In anchor-free environments, methods with reliable accuracy for a long-distance navigation are required [37]. Some works on terrestrial anchor-free scenarios have been carried out for WSNs [38]. However, many of them only consider static scenarios, and the algorithms cannot be directly used in underwater environments. As for underwater anchor-free scenarios, [39] and [40] use neural networks and terrain-aided methods to overcome the accumulated inertial errors, respectively. However, the work merely focuses on the single-AUV navigation problems. A flow-aided method is proposed in [41], in which the involvement of flow information leads to a better localization performance than that of DR. Nevertheless, in the proposed methods, cooperation is achieved only in an opportunistic manner. The anchor-free localization methods in [42] are only applied in statical underwater WSNs where the sensor nodes that need localization are anchored to the seafloor with hemispherical position uncertainties.

In this article, we investigate the range-based multi-AUV CL issues in anchor-free scenarios. Our goal is to alleviate the impacts of the accumulated inertial measurement errors and slow down the growth of the localization error. As a result, AUVs are able to navigate underwater for a long time with good localization accuracy. We provide a distributed solution with an intermittent CL framework named intermittent belief propagation based dead reckoning (IBPDR). Under the IBPDR framework, we further design the underwater-adaptive belief propagation (UABP) CL algorithm and the particle-based current-aided filter (PCAF), which are used, respectively, in different parts of IBPDR to improve the localization performance. The main contributions of this article are summarized as follows.

1) We develop an IBPDR framework, in which cooperations among AUVs happen intermittently. In this way, the interaction frequency among AUVs is decreased. Thus, the communication costs are reduced. In addition, when no cooperation happens, noncooperative localization methods, such as terrain-aided [40] or flow-aided [41] methods, could be implemented. Such algorithms bring in more useful information to assist localization. The framework provides a natural combination of cooperative and noncooperative methods.
2) We propose a particle-based CL algorithm named UABP. It has inherited the advantages of the standard BP, such as distributed estimation, less complexity, and good scalability. Meanwhile, the merits of the particle-based BP, such as the feasibility in nonlinear non-Gaussian cases and the ability of providing estimation uncertainties, also exist in UABP. To make UABP suitable for our multi-AUV CL problems, the following modifications are made. First, instead of the direct use of the inertial measurements to predict AUVs' positions, we design a position prediction process considering the accumulated errors contained in the inertial measurements. Hence, the obtained prior position distributions of AUVs' are able to alleviate the effect of the accumulated errors in the later fusion processes of UABP. Second, we minimize the transmitted data volume to a position vector and an uncertainty parameter. In this way, compared with transmitting hundreds of particles, UABP only requires the transmission of three real numbers between two AUVs at one interaction. Third, the number of iterations in UABP is restricted to one. The reduction of iterations reduces the communication costs as well as prevents the overconfident estimation problem in multi-iteration methods [23].
3) We propose the PCAF to further improve the localization accuracy when no cooperation among AUVs happens. The PCAF has a position prediction process similar to that in UABP and brings useful current information into the framework without increasing the communication cost.

The rest of this article is organized as follows. The system model is presented in Section II. An overview of BP-based CL methods and the proposed methods are described in Sections III and IV, respectively. In Section V, simulation examples are presented and analyzed to show the advantages of the proposed methods. The conclusions are delivered in Section VI.

II. System Model

In this article, we investigate the localization of a team of AUVs in anchor-free environments. The definition of "anchor-free" is that AUVs cannot receive GPS signals (or something alike) and obtain localization assistance from devices with known absolute positions during navigations. As we all know, the underwater environment is three-dimensional (3-D). However, when AUVs are carrying out a task, they usually navigate in a fixed depth. In addition, current underwater devices are always equipped with depth sensors, due to which the depth information can be assumed known all the time. Thus, in our scenario, a 2-D localization problem is discussed with the coordinates of the ith AUV at the time t modeled as $\boldsymbol{x}_i^{(t)} = [\alpha_i^{(t)}, \beta_i^{(t)}]^T$. Note that, in this article, we use the bold symbol $\boldsymbol{x}$ (or $\boldsymbol{y}$) and the Roman symbol $\mathbf{x}$ (or $\mathbf{y}$) to denote variable and particle vectors, respectively. The symbol $\mathbf{y}$ is used when introducing the pure mathematical techniques, and the symbol $\mathbf{x}$ is used when discussing AUV CL issues. In addition, the time index (represented by timestep hereafter) and the AUV index appear in the superscript and subscript of the symbols, respectively.

In the later discussions, we assume that the deployment positions (the start positions of the navigation) of AUVs are exactly known to exclude the impact of the initial localization error. We also assume AUVs are equipped with inertial navigation sensors, such as IMUs, and acoustic modems with ranging and communication abilities. In modern underwater vehicles (especially AUVs), both IMUs and acoustic modems have become common [4], even for small-sized AUVs [43]. The available measurements for localization are with two kinds: the inertial (proprioceptive) measurements and the inter-AUV measurements.

The inertial measurements are the speed ($\hat{v}_i^{(t)}$) and the heading angle ($\hat{\theta}_i^{(t)}$) of the ith AUV directly measured from the inertial navigation sensors including several kinds of noises [44]. They are the basic information for the position evolution of AUVs between different timesteps.

For the inter-AUV measurements, we model the measured inter-AUV distance at timestep t as

$$\hat{d}_{j\to i}^{(t)} = d_{j\to i}^{(t)} + \nu_{j\to i}^{(t)} \tag{1}$$

$$= \left\| \boldsymbol{x}_j^{(t)} - \boldsymbol{x}_i^{(t)} \right\|_2 + \nu_{j\to i}^{(t)} \tag{2}$$

where $\hat{d}_{j\to i}^{(t)}$ indicates the distance between the jth and the ith AUVs measured at the ith AUV, $d_{j\to i}^{(t)}$ is the true distance with $d_{j\to i}^{(t)} = d_{i\to j}^{(t)}$, $\boldsymbol{x}_j^{(t)}$ denotes the coordinates of the jth AUV, and $\nu_{j\to i}^{(t)}$ is the measurement noise with variance $\sigma^2_{r,j\to i}$. The corresponding bearing $\hat{\phi}_{j\to i}^{(t)}$ of the measured distance $\hat{d}_{j\to i}^{(t)}$ is modeled as

$$\hat{\phi}_{j\to i}^{(t)} = \phi_{j\to i}^{(t)} + \xi_{j\to i}^{(t)} \tag{3}$$

where $\phi_{j\to i}^{(t)}$ is the true bearing and $\xi_{j\to i}^{(t)}$ is the measurement noise with variance $\sigma^2_{b,j\to i}$. In this article, we assume that different inter-AUV distance (or bearing) measurements $\hat{d}_{j\to i}^{(t)}$ and $\hat{d}_{j'\to i'}^{(t)}$ (or $\hat{\phi}_{j\to i}^{(t)}$ and $\hat{\phi}_{j'\to i'}^{(t)}$) are independent from each other unless $j = j'$ and $i = i'$.

III. CL Using BP

BP [45], [46] is based on graphical models [47], which are widely used in inference problems. A graph $\mathcal{G} = (\mathcal{V}, \mathcal{E})$ usually consists of a node set $\mathcal{V}$ and an edge set $\mathcal{E}$. In AUV localization, each node $i \in \mathcal{V}$ indicates an AUV associated with a position variable $\boldsymbol{x}_i^{(t)}$. Each edge $(i, j) \in \mathcal{E}$ denotes the existence of the interactions between two AUVs. With all the AUV nodes and edges, the specific structure of the graph $\mathcal{G}$ can represent a joint probability density function (PDF) of all position variables.

Based on the Hammersley–Clifford theorem [48], the joint posterior PDF of all AUVs can be represented by the likelihood functions of the inter-AUV measurements $p(\hat{d}_{j\to i}^{(t)}, \hat{\phi}_{j\to i}^{(t)} | \boldsymbol{x}_j^{(t)}, \boldsymbol{x}_i^{(t)})$ and the prior position distributions $p_{pri}(\boldsymbol{x}_i^{(t)})$ of AUVs

$$p(\boldsymbol{X}^{(t)}|\boldsymbol{O}^{(t)}) = \prod_{(i,j)\in\mathcal{E}} p\left(\hat{d}_{j\to i}^{(t)}, \hat{\phi}_{j\to i}^{(t)} | \boldsymbol{x}_j^{(t)}, \boldsymbol{x}_i^{(t)}\right) \prod_{i\in\mathcal{V}} p_{pri}\left(\boldsymbol{x}_i^{(t)}\right) \tag{4}$$

where $\boldsymbol{X}^{(t)}$ collects all $\boldsymbol{x}_i^{(t)}, i = 1, \ldots, N$, with N is the number of AUVs in the AUV team, and $\boldsymbol{O}^{(t)} = \{\hat{d}_{j\to i}^{(t)}, \hat{\phi}_{j\to i}^{(t)} : i, j \in \mathcal{V}, (i, j) \in \mathcal{E}\}$ indicates all the noisy inter-AUV measurements. The prior position distribution $p_{pri}(\boldsymbol{x}_i^{(t)})$ is evolved from the position at the last timestep

$$p_{pri}\left(\boldsymbol{x}_i^{(t)}\right) = p\left(\boldsymbol{x}_i^{(t)} | \boldsymbol{x}_i^{(t-1)}, \boldsymbol{Q}_i^{(t-1)}\right), \quad i \in \mathcal{V} \tag{5}$$

with inertial measurements indicated by $\boldsymbol{Q}_i^{(t-1)} = \{\hat{v}_i^{(t-1)}, \hat{\theta}_i^{(t-1)} : i \in \mathcal{V}\}$. Similar position prediction methods have been applied in [40].

To localize an AUV, an estimate $\hat{\boldsymbol{x}}_i^{(t)}$ of the position variable $\boldsymbol{x}_i^{(t)}$ is expected. Note that we have already obtained the joint posterior PDF of all position variables. If we can obtain the marginal posterior distribution of $\boldsymbol{x}_i^{(t)}$, the estimated value $\hat{\boldsymbol{x}}_i^{(t)}$ could be easily calculated by the Bayesian estimators, such as the minimum mean squared error (MMSE) estimator (or the maximum posterior estimator) [21]

$$\hat{\boldsymbol{x}}_{i,\mathrm{MMSE}}^{(t)} = \int \boldsymbol{x}_i^{(t)} p\left(\boldsymbol{x}_i^{(t)} | \boldsymbol{O}^{(t)}\right) d\boldsymbol{x}_i^{(t)}. \tag{6}$$

However, the straightforward way of calculating the marginal posterior distribution is integrating the joint posterior PDF over all variables except $\boldsymbol{x}_i^{(t)}$

$$p\left(\boldsymbol{x}_i^{(t)} | \boldsymbol{O}^{(t)}\right) = \int p\left(\boldsymbol{X}^{(t)} | \boldsymbol{O}^{(t)}\right) d\boldsymbol{X}^{(t)} \backslash \boldsymbol{x}_i^{(t)} \tag{7}$$

where $\boldsymbol{X}^{(t)} \backslash \boldsymbol{x}_i^{(t)}$ denotes all variables in $\boldsymbol{X}^{(t)}$ except $\boldsymbol{x}_i^{(t)}$. Although the idea is straightforward, the total computational amount increases exponentially as the AUV team grows in size. Thus, we resort to BP to calculate the marginal posterior distribution in an efficient way.

BP is an iterative message-passing algorithm that is able to efficiently calculate the marginal posterior distribution of each AUV's position variable in a distributed manner. Its whole computational amount is only proportional to the number of AUVs. In BP, the calculated *belief* is an approximation of the marginal posterior distribution.

To illustrate BP, the definitions of the *message* and *belief* go first. The *message* is the information transmitted from one AUV to another. Let us take $\boldsymbol{N}(i) = \{j \in \mathcal{V} | (i, j) \in \mathcal{E}\}$ as the set of neighboring AUVs of the ith AUV. Then, the *message* from its neighbor $j \in \boldsymbol{N}(i)$ to the ith AUV at the iteration l is given by [21]

$$m_{j\to i}^{l}\left(\boldsymbol{x}_i^{(t)}\right) \propto \int p\left(\hat{d}_{j\to i}^{(t)}, \hat{\phi}_{j\to i}^{(t)} | \boldsymbol{x}_j^{(t)}, \boldsymbol{x}_i^{(t)}\right) b_j^{l-1}\left(\boldsymbol{x}_j^{(t)}\right) d\boldsymbol{x}_j^{(t)}. \tag{8}$$

In AUV localization, the *message* $m_{j\to i}^{l}(\boldsymbol{x}_i^{(t)})$ denotes the relative position information about the ith AUV, taking the jth AUV as the reference. Once all the *messages* from the neighbors have been received by the ith AUV, its *belief* can be easily obtained

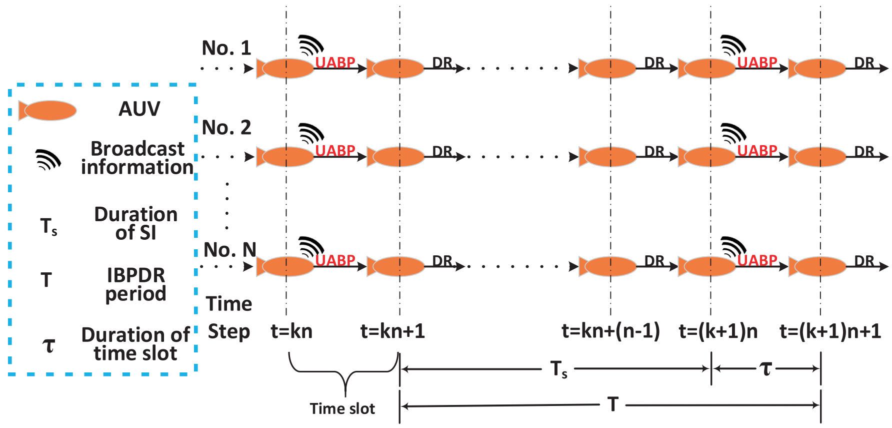

Fig. 1. Proposed IBPDR framework: Each AUV uses DR to estimate its position in the SI and the UABP localization algorithm in the correction timesteps.

by multiplying all the incoming *messages* with the local prior position distribution

$$b_i^l\left(\boldsymbol{x}_i^{(t)}\right) \propto p_{pri}\left(\boldsymbol{x}_i^{(t)}\right) \prod_{j\in \boldsymbol{N}(i)} m_{j\to i}^l\left(\boldsymbol{x}_i^{(t)}\right). \tag{9}$$

With the clarity of the *message* and *belief*, the process of BP is very simple. During every iteration, every AUV calculates *messages* and sends them to its neighbors. Meanwhile, it receives *messages* from the neighbors and calculates its own *belief*. After sufficient iterations, the *belief* of each AUV will converge to the exactly marginal distribution (for tree-structured graphs) or an approximation of the marginal distribution in most cases (for graphs with loops) [22], [29].

The particle-based BP is an important variant of BP. It has been extensively applied to localization problems over WSNs [28], [29]. The main idea is to use groups of weighted particles to represent the *beliefs* and *messages*. In localization, non-Gaussian and nonlinear cases extensively exist [28] and make the standard BP infeasible. One merit of the particle-based BP is that it is naturally accessible to both nonlinear and non-Gaussian cases. Moreover, the particle-based BP can provide estimates as well as the corresponding estimation uncertainties. Due to the above advantages of the particle-based BP, the proposed methods in Section IV are all particle-based.

IV. Underwater Anchor-Free CL Algorithm

Due to the complexity of underwater environments, the terrestrial localization algorithms cannot be directly used underwater. In this article, according to the requirements of multi-AUV navigation, we design particle-based algorithms that are suitable for underwater applications. In this section, the proposed methods are described in detail.

A. Anchor-Free Intermittent CL Framework

In anchor-free environments, without any anchor (absolute reference), AUVs use DR for self-localization. However, the unbounded growth of DR's localization error leads to very low localization accuracy for long-time navigations. Thus, a correction of DR's error is needed. The goal of our work is to periodically correct DR's error with CL among AUVs. As a result, the error growth of DR is slowed down and AUVs are able to stay underwater for a much longer time. Hence, we propose an intermittent CL framework named IBPDR. In IBPDR, the proposed UABP CL algorithm is applied to localize AUVs once in a period as a correction to DR's deviation. The general process of IBPDR is shown in Fig. 1.

According to Fig. 1, we first define $T = n\tau$ as the period of IBPDR, which includes n equal-length time slots (the duration between two consecutive timesteps) with length τ. During every IBPDR period, AUVs use DR for self-localization in the first $(n-1)$ time slots and apply UABP to cooperatively localize themselves in the last time slot. Since no communication happens among AUVs during the first $(n-1)$ time slots, we name this duration $T_s = (n-1)\tau$ as the silent interval (SI). To achieve such a time division, we assume that AUVs are synchronized with each other. Related works for synchronization have been investigated in [22] and [49].

The existence of the SI is the reason that IBPDR is an intermittent framework. An important advantage of IBPDR is that it reduces the communication costs over the AUV team by decreasing the communication frequency to once a period. In WSNs applications, reducing the energy consumption is crucial in practice, and it is more relevant underwater. Another advantage of IBPDR is that some noncooperative methods could be implemented during the SI, so that cooperative and noncooperative methods can be properly combined under the framework to jointly improve the localization accuracy of AUVs. The designed PCAF (introduced in Section IV-D) is an example of using noncooperative methods as a complement in the SI. The good scalability of IBPDR provides possibilities for further improvements.

For clarity in the following sections, we define three sets of timesteps $\mathcal{T}^{\mathrm{C}}$, $\mathcal{T}^{\mathrm{NC}}$, and $\mathcal{T}$

$$\mathcal{T}^{\mathrm{C}} = kn, \quad k \in \mathbb{N}^+ \tag{10}$$

$$\mathcal{T}^{\mathrm{NC}} = \bigcup_{k\in\mathbb{N}} \{kn+1, \ldots, kn+(n-1)\} \tag{11}$$

$$\mathcal{T} = \mathcal{T}^{\mathrm{C}} \bigcup \mathcal{T}^{\mathrm{NC}}. \tag{12}$$

Timestep $t \in \mathcal{T}^{\mathrm{C}}$ (or $\mathcal{T}^{\mathrm{NC}}$) means that AUVs use cooperative (or noncooperative) methods for localization in the time slot between the timesteps t and $(t+1)$.

B. Inertial Localization and DR

Inertial localization can be defined as an AUV using continuously measured inertial data (the heading angles and the speeds) to estimate its positions. The estimation principle is always DR. With the knowledge of the previous position $\boldsymbol{x}_i^{(t-1)} = [\alpha_i^{(t-1)}, \beta_i^{(t-1)}]^T$ and the measurements from IMUs ($\hat{\theta}_i^{(t-1)}$ and $\hat{v}_i^{(t-1)}$), an AUV can easily calculate its current position $\boldsymbol{x}_i^{(t)} = [\alpha_i^{(t)}, \beta_i^{(t)}]^T$ with DR

$$\boldsymbol{x}_i^{(t)} = \boldsymbol{x}_i^{(t-1)} + \hat{v}_i^{(t-1)}\tau \left[\sin\hat{\theta}_i^{(t-1)};\, \cos\hat{\theta}_i^{(t-1)}\right] \tag{13}$$

where t and $(t-1)$ indicates the timesteps.

The convenience and high stability of DR make it the most fundamental method for AUV self-localization. However, its accumulated error grows without bound [4].

C. Underwater-Adaptive Belief Propagation

BP has been widely used in CL for WSNs. However, terrestrial algorithms cannot be directly applied underwater. Some adaptations according to the underwater characteristics should be considered. In this section, we propose a particle-based variant of BP called UABP. Its design is based on the basic principles of BP message-passing scheme described in Section III. The main modifications in UABP focus on alleviating the impact of the accumulated errors and reducing the transmitted data volume among AUVs. Note that, during AUV navigation, only inertial measurements with accumulated errors are available. Our work provides a proper way to apply the obtained inertial measurements to alleviate the impact of the unknown accumulated errors. Moreover, the speed measurements can be obtained from other navigation sensors with higher accuracy, such as the Doppler velocity log, and the errors in the heading angle can cause major impact on 2-D position estimation [44]. Thus, we assume that the accumulated errors in the speed measurements are smaller than those in the heading angle measurements.

In UABP, the calculation of the *belief* is the key for localization. To calculate the *belief*, let us recall (9). The *belief* of an AUV is a product of the prior position distribution (termed the *prior* hereafter) and all the received *messages*. Since UABP is particle-based, in the following paragraphs, we will introduce how we use particles to obtain the *prior* and the *messages* and how to perform the multiplication. Note that the particles we use have many notations, and their meanings are listed in Table I.

1) Prior: In AUV localization algorithms, a prediction of the position as the prior position information at the current timestep is required. It is usually performed by DR. Due to the error accumulation in DR, we do not use it to perform prediction. We propose a particle-based position prediction method to generate the *prior* with all the inertial measurements between two correction timesteps and the output *belief* in the previous correction

TABLE I
MEANING OF NOTATIONS

Location	Notation	Meaning
Superscript	(t)	Timestep
First subscript	pri	*Prior*
	b	*Belief*
	m	*Message*
	p	*Proposal*
Second subscript	k	Particle index
Third subscript	i, j	AUV index
	$j \to i$	Information transmitted from j to i

timestep. Thus, (5) is rewritten as

$$p_{pri}\left(\boldsymbol{x}_i^{(t)}\right) = p\left(\boldsymbol{x}_i^{(t)} | \boldsymbol{x}_i^{(t-n)}, \boldsymbol{Q}_i^{(t-n:t-1)}\right) \tag{14}$$

where $\boldsymbol{Q}_i^{(t-n:t-1)}$ includes all the inertial measurements from the timestep $(t-n)$ to $(t-1)$.

Suppose that the *prior* of the ith AUV in the current timestep $t \in \mathcal{T}^C$ is $p_{pri}(\boldsymbol{x}_i^{(t)})$, represented by weighted particles $\boldsymbol{P}_i^{(t)} = \{\mathbf{x}_{pri,k,i}^{(t)}, w_{pri,k,i}^{(t)}\}_{k=1}^K$ and the output *belief* of the ith AUV in the previous correction timestep $(t-n) \in \mathcal{T}^C$ is $b(\boldsymbol{x}_i^{(t-n)})$, represented by weighted particles $\boldsymbol{B}_i^{(t-n)} = \{\mathbf{x}_{b,k,i}^{(t-n)}, w_{b,k,i}^{(t-n)}\}_{k=1}^K$. The position prediction functions are as follows:

$$\begin{aligned}\mathbf{x}_{pri,k,i}^{(t)} &= \mathbf{x}_{b,k,i}^{(t-n)} + v_{k,i}^{(t-n)}\tau\left[\sin\left(\theta_{k,i}^{(t-n)}\right);\, \cos\left(\theta_{k,i}^{(t-n)}\right)\right] \\ &\quad + \cdots + v_{k,i}^{(t-1)}\tau\Big[\sin\Big(\theta_{k,i}^{(t-1)}\Big);\, \cos\Big(\theta_{k,i}^{(t-1)}\Big)\Big],\, v_{k,i}^{(t-m)} \\ &\quad \sim \mathcal{N}\left(\hat{v}_i^{(t-m)}, {\sigma_{v,i}^{(t-m)}}^2\right), \quad \theta_{k,i}^{(t-m)} \\ &\quad \sim \mathcal{N}\left(\hat{\theta}_i^{(t-m)},\, {\sigma_{\theta,i}^{(t-m)}}^2\right), \quad m = 1, 2, \ldots, n\end{aligned} \tag{15}$$

$$w_{pri,k,i}^{(t)} = w_{b,k,i}^{(t-n)} \tag{16}$$

where $\sigma_{v,i}^{(t-m)}$ is the uncertainty of the speed measurements, and $\sigma_{\theta,i}^{(t-m)} = \sigma_{\theta,i}^{(t-m-1)} + \Delta\sigma_{\theta,i}$ indicates the accumulated uncertainty of the heading angle measurements, respectively. The measured speed $\hat{v}_i^{(t-m)}$ and heading angle $\hat{\theta}_i^{(t-m)}$ of the ith AUV are from the measured speed set $\boldsymbol{V}_i^{(t-1)} = \{\hat{v}_i^{(t-n)}, \ldots, \hat{v}_i^{(t-1)}\}$ and the measured heading angle set $\boldsymbol{\Theta}_i^{(t-1)} = \{\hat{\theta}_i^{(t-n)}, \ldots, \hat{\theta}_i^{(t-1)}\}$, respectively.

If AUVs move along straight trajectories with constant speeds, (15) can be simplified as

$$\begin{aligned}\mathbf{x}_{pri,k,i}^{(t)} &= \mathbf{x}_{b,k,i}^{(t-n)} + v_{k,i}T\left[\sin(\theta_{k,i});\, \cos(\theta_{k,i})\right], \\ v_{k,i} &\sim \mathcal{N}\left(\bar{v}_i,\, {\sigma_{v,i}^{(t-1)}}^2\right), \quad \theta_{k,i} \sim \mathcal{N}\left(\bar{\theta}_i,\, {\sigma_{\theta,i}^{(t-1)}}^2\right)\end{aligned} \tag{17}$$

where $\bar{v}_i$ and $\bar{\theta}_i$ are the means of the measured speeds in $\boldsymbol{V}_i^{(t-1)}$ and heading angles in $\boldsymbol{\Theta}_i^{(t-1)}$, respectively. Since every particle is treated equally in this procedure, its corresponding weight

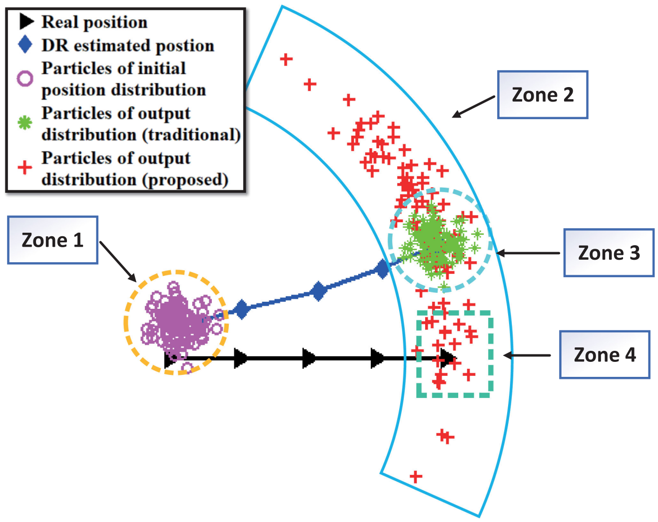

Fig. 2. Position prediction: Magenta dots in Zone 1 are the estimated position distribution at the former timestep. Red crosses and green asterisks in Zone 2 and 3 are the output distributions of the proposed and traditional position prediction methods, respectively. Zone 4 is the ideal place in which particles can provide good estimations.

remains unchanged. In this way, we have obtained the weighted particles $\boldsymbol{P}_i^{(t)} = \{\mathbf{x}_{pri,k,i}^{(t)}, w_{pri,k,i}^{(t)}\}_{k=1}^{K}$ of the *prior*.

In (15), we do not use the measured heading angles $\hat{\theta}_i^{(t-m)}$ directly, but use particles sampled from a Gaussian distribution centered by the measured heading angle with the accumulated uncertainty. The goal of this design is trying to provide a way to use the inertial measurements properly and alleviate the impact of the accumulated errors in the inertial measurements. As a result, the obtained *prior* can cover the true position of the AUV even when the accumulated errors are large. This is important for obtaining a good estimate in the later fusion of UABP. The accumulated uncertainty $\sigma_{\theta,i}^{(t-m)}$ can also be rewritten as $\sigma_{\theta,i}^{(t-m)} = \sigma_{\theta,i}^{(1)} + (t-m-1)\Delta\sigma_{\theta,i}$, where $\sigma_{\theta,i}^{(1)}$ is the uncertainty of the measurement at the beginning of the navigation. In real-world applications, $\sigma_{\theta,i}^{(1)}$ is usually small and can be approximated to zero. It is because the inertial navigation sensors should be calibrated before the AUV deployment and the errors are not accumulated over time yet. The reasons we design the accumulated uncertainty $\sigma_{\theta,i}^{(t-m)}$ are as follows. The accumulated errors in the inertial measurements are the mixtures of different kinds of errors. They contain several kinds of error sources [44], such as the constant bias, the angle random walk, etc. In addition, different kinds of errors have different statistic characteristics. For example, the angular error of a constant bias grows linearly with time, and the standard deviation of the angle random walk grows proportionally to the square root of time. Thus, the statistics of the accumulated errors are difficult to describe. However, the errors will definitely grow with time as well as the error uncertainties. By designing the accumulated uncertainty, we can approximate the accumulation and the deviation of the inertial measurement errors. Fig. 2 shows the basic idea of the proposed particle-based position prediction.

In Fig. 2, the black and the blue lines are the real and the DR estimated trajectories, respectively. Both lines are composed of four parts, meaning time spans four timesteps. Note that the trajectories are only a small part of the whole movement path. Therefore, the beginning of the lines are not overlapped, meaning the existence of localization error. The particles are represented by different markers. In Fig. 2, the magenta particles in Zone 1 represent the initial position distribution. In the traditional position prediction, such as DR, the inertial measurements are directly used on the particles in Zone 1 to obtain the prediction with the output particles (green asterisks) appear in Zone 3. It can be expressed as

$$\mathbf{x}_{pri,k,i}^{(t)} = \mathbf{x}_{b,k,i}^{(t-n)} + \hat{v}_i^{(t-n)}\tau\left[\sin\left(\hat{\theta}_i^{(t-n)}\right); \cos\left(\hat{\theta}_i^{(t-n)}\right)\right] + \cdots + \hat{v}_i^{(t-1)}\tau\left[\sin\left(\hat{\theta}_i^{(t-1)}\right); \cos\left(\hat{\theta}_i^{(t-1)}\right)\right]. \tag{18}$$

Obviously, all the green particles are far from the real trajectory (the black line). In such a situation, the estimation cannot be good. Although the position prediction only provides the *prior*, it is important that there are particles near the real position. Therefore, we would prefer particles in Zone 4. Red particles in Zone 2 is the output of our proposed position prediction method. We can see that Zone 2 contains Zone 4. What we need to do is to filter the particles in Zone 4 out of Zone 2 in the later operations.

2) Message: Recalling (8), the *message* is related to the received *beliefs* from the transmitting AUVs and the pairwise relationship between the transmitting and receiving AUVs. Since each AUV has a prior position information of itself, one iteration of message passing among AUVs is enough for each AUV to obtain a position estimate. Thus, we limit the number of iterations in UABP to one. In this way, the communication costs are reduced with only one iteration of message passing. Moreover, the overconfident problem is avoided [50]. Because the *messages* received by an AUV from its neighbors are not correlated with its own broadcasted *belief*, thus we rewrite (8) as

$$m_{j\to i}^{(t)}(\boldsymbol{x}_i^{(t)}) \propto \int p\left(\hat{d}_{j\to i}^{(t)}, \hat{\phi}_{j\to i}^{(t)} | \boldsymbol{x}_j^{(t)}, \boldsymbol{x}_i^{(t)}\right) b_j^{(t)}\left(\boldsymbol{x}_j^{(t)}\right) d\boldsymbol{x}_j^{(t)} \tag{19}$$

where the superscript is the time index instead of the iteration index.

We first explain the composition of the transmitted *belief* ($b_j^{(t)}(\boldsymbol{x}_j^{(t)})$ in (19)). Since the *beliefs* are in the form of particles, we define the *belief uncertainty* of the jth AUV at the timestep t as $U_j^{(t)}$ to indicate the uncertainty of the particles. Note that, at the *belief*-broadcasting stage of UABP, new *beliefs* at timestep t have not been computed yet, and $U_j^{(t)}$ is defined on the output *beliefs* $\boldsymbol{B}_j^{(t-n)} = \{\mathbf{x}_{b,k,j}^{(t-n)}, w_{b,k,j}^{(t-n)}\}_{k=1}^{K}$ at the previous cooperation timestep $(t-n) \in \mathcal{T}^C$

$$U_j^{(t)} = \sum_{k=1}^{K} w_{b,k,j}^{(t-n)} \left\|\mathbf{x}_{b,k,j}^{(t-n)} - \bar{\mathbf{x}}\right\|_2^2 \tag{20}$$

where $\bar{\mathbf{x}} = \sum_{k=1}^{K} w_{b,k,j}^{(t-n)} \mathbf{x}_{b,k,j}^{(t-n)}$. When the jth AUV broadcasts its *belief*, only its current position and the *belief uncertainty* $U_j^{(t)}$ are transmitted. However, at this stage, no position estimate is generated by CL yet. The jth AUV transmits its predicted position $\boldsymbol{x}_j^{-(t)}$ calculated by DR with (13). At the receiving AUV i, a Gaussian distribution $\mathcal{N}(\boldsymbol{x}_j^{-(t)}, \mathbf{C}_j^{(t)})$ is used to approximate the received *belief*, where $\mathbf{C}_j^{(t)} = \mathrm{diag}\{U_j^{(t)}, U_j^{(t)}\}$. Hence, particles are directly sampled from $\mathcal{N}(\boldsymbol{x}_j^{-(t)}, \mathbf{C}_j^{(t)})$ to form the particle representation of the received *belief*. Such a parametric approximation reduces the transmitted data volume from a set of particles to only two parameters.

Here, we assume that the *belief* of the transmitting AUV j is represented by K weighted particles $\boldsymbol{B}_j^{-(t)} = \{\mathbf{x}_{b,k,j}^{-(t)}, w_{b,k,j}^{-(t)}\}_{k=1}^{K}$. As for the pairwise relationship, it is denoted by the measured inter-AUV distance $\hat{d}_{j\to i}^{(t)}$ with corresponding bearing $\hat{\phi}_{j\to i}^{(t)}$. Then, the particle representation $\boldsymbol{M}_{j\to i}^{(t)} = \{\mathbf{x}_{m,k,j\to i}^{(t)}, w_{m,k,j\to i}^{(t)}\}_{k=1}^{K}$ of the *message* from the jth AUV to the ith AUV can be calculated by

$$\mathbf{x}_{m,k,j\to i}^{(t)} = \mathbf{x}_{b,k,j}^{-(t)} + d_k^{(t)} \left[\sin\left(\phi_k^{(t)}\right); \cos\left(\phi_k^{(t)}\right) \right],$$
$$d_k^{(t)} \sim \mathcal{N}\left(\hat{d}_{j\to i}^{(t)}, \sigma_{r,j\to i}^2\right), \phi_k^{(t)} \sim \mathcal{N}\left(\hat{\phi}_{j\to i}^{(t)}, \sigma_{b,j\to i}^2\right) \tag{21}$$

$$w_{m,k,j\to i}^{(t)} = w_{b,k,j}^{-(t)} \tag{22}$$

where $\sigma_{r,j\to i}^2$ and $\sigma_{b,j\to i}^2$ are the variances of the inter-AUV measurements defined in Section II. Since all the particles in $\boldsymbol{B}_j^{-(t)}$ are equally treated, the weights remain unchanged.

3) Multiplication and Position Estimation: We now have described the particle representations of the *prior* and the *message*. According to (9), to calculate the *belief*, a multiplication procedure should be carried out. Because the *prior* and the incoming *messages* are all in the form of weighted particles, the kernel density estimation (KDE) [51] is applied here to form the particles into distributions. Assuming a particle set $\{\mathbf{y}_k, \omega_k\}_{k=1}^{K}$ represents distribution $p(\boldsymbol{y})$ with particles $\mathbf{y}_k$ and corresponding weights ω_k, the KDE of $p(\boldsymbol{y})$ is

$$\hat{p}(\boldsymbol{y}) = \sum_{k=1}^{K} \omega_k K_h(\boldsymbol{y} - \mathbf{y}_k) \tag{23}$$

where

$$K_h(\boldsymbol{y}) = \frac{1}{(\sqrt{2\pi}h)^M} \exp\left(-\frac{\|\boldsymbol{y}\|^2}{2h^2}\right) \tag{24}$$

is the Gaussian kernel with a bandwidth h equal to the standard deviation of the ranging measurements [52] and M is the dimension of $\boldsymbol{y}$ in (24).

Let us define the KDEs of the *prior* of the ith AUV as $\hat{p}_{pri}(\boldsymbol{x}_i^{(t)})$ and the incoming *message* from the jth AUV to the ith AUV as $\hat{m}_{j\to i}(\boldsymbol{x}_i^{(t)})$, respectively. The product of these KDEs

Algorithm 1: UABP CL Algorithm at Timestep t.

AUVs $i = 1$ to N **in parallel**
- broadcast DR position estimation $\boldsymbol{x}_i^{-(t)}$ and *belief uncertainty* $U_i^{(t)}$
- receive $\boldsymbol{x}_j^{-(t)}$ and $U_j^{(t)}$ from neighbors, $j \in \boldsymbol{N}(i)$
- convert $\boldsymbol{x}_j^{-(t)}$ and $U_j^{(t)}$ to Gaussian distributions as received *beliefs*
- draw K i.i.d. particles from each received *belief* as $\boldsymbol{B}_j^{-(t)}$
- compute $\boldsymbol{M}_{j\to i}^{(t)}$ according to (21) and (22) , $j \in \boldsymbol{N}(i)$
- compute $\boldsymbol{P}_i^{(t)}$ according to (15) and (16)
- draw K particles from the *proposal* and compute corresponding weights according to (26)
- normalize the weights and get $\boldsymbol{D}_i^{(t)}$
- compute $\boldsymbol{B}_i^{(t)}$ by resampling (with replacement) $\boldsymbol{D}_i^{(t)}$
- compute the new position estimation $\hat{\boldsymbol{x}}_{i,\mathrm{MMSE}}^{(t)}$ according to (28)
- compute $U_i^{(t+n)}$ according to (20) for the application of UABP at timestep $(t+n) \in \mathcal{T}^C$

end parallel

is as follows:

$$P(\boldsymbol{x}_i^{(t)}) = \hat{p}_{pri}\left(\boldsymbol{x}_i^{(t)}\right) \prod_{j\in\boldsymbol{N}(i)} \hat{m}_{j\to i}\left(\boldsymbol{x}_i^{(t)}\right). \tag{25}$$

To estimate the *belief*, we need to draw particles from (25). Since each KDE of a *message* or the *prior* is a weighted summation of K Gaussian distributions, the closed form of the product of KDEs in (25) is difficult to obtain. Thus, the direct sampling of (25) is usually infeasible. In this way, importance sampling [53] becomes a solution. We first draw K particles $\{\mathbf{x}_{p,k,i}^{(t)}\}_{k=1}^{K}$ from a proposal distribution (termed the *proposal* hereafter) $q(\cdot)$ and then weight each particle by

$$w_{p,k,i}^{(t)} \propto \frac{P\left(\mathbf{x}_{p,k,i}^{(t)}\right)}{q\left(\mathbf{x}_{p,k,i}^{(t)}\right)}. \tag{26}$$

After normalization, the particle set $\boldsymbol{D}_i^{(t)} = \{\mathbf{x}_{p,k,i}^{(t)}, w_{p,k,i}^{(t)}\}_{k=1}^{K}$ could be the representation of the ith AUV's *belief*. Usually, a resample operation is needed to deal with the sample depletion [54], which is a common problem in particle-based methods. To perform resampling, we independently draw K particles (with replacement) from $\boldsymbol{D}_i^{(t)}$ with the selected probability of each particle in $\boldsymbol{D}_i^{(t)}$ equals to its corresponding weight. As a result, we obtain K equally weighted particles $\boldsymbol{B}_i^{(t)} = \{\mathbf{x}_{b,k,i}^{(t)}, w_{b,k,i}^{(t)}\}_{k=1}^{K}$ as the output *belief* of the ith AUV.

In this method, the choice of the *proposal* is very important. In general, the whole multiplication process can be viewed as resampling from the *proposal*. Since the *prior* and the *messages* all indicate the position information about the ith AUV based on the inertial and inter-AUV measurements, the overlapping region of them should be near the true position of the ith AUV. During the multiplication, the particles in this region (see Zone 4 in Fig. 2) are more likely to obtain high weights when the weights are calculated according to (26). After normalization and resample operations, these particles will become dominant in the particle set. In this way, with most particles near the true position, a good estimate with (28) is easy to obtain. In UABP, we choose the *prior* to be the *proposal*. Then, the corresponding weights of particles $\{\mathbf{x}_{p,k,i}^{(t)}\}_{k=1}^{K}$ can be calculated by

$$w_{p,k,i}^{(t)} \propto \prod_{j\in \boldsymbol{N}(i)} \hat{m}_{j\to i}\left(\mathbf{x}_{p,k,i}^{(t)}\right). \tag{27}$$

We have now obtained the *belief* of the ith AUV using UABP. Since the *belief* is an approximation of the marginal posterior distribution of the position variable $\boldsymbol{x}_i^{(t)}$, the estimated position $\hat{\boldsymbol{x}}_i^{(t)}$ can be easily achieved by the MMSE estimator

$$\hat{\boldsymbol{x}}_{i,\text{MMSE}}^{(t)} = \sum_{k=1}^{K} w_{b,k,i}^{(t)}\mathbf{x}_{b,k,i}^{(t)}. \tag{28}$$

The proposed UABP localization algorithm is shown in **Algorithm 1**

D. Improvements in SI

The basic rule in the SI is that no communication happens among AUVs. Without cooperation, AUVs use only DR to update their positions. In this way, performance degradation is inevitable. In such circumstance, the design of noncooperative methods with extra useful information may improve the localization accuracy in the SI and, in turn, the IBPDR framework. However, such information or methods are not easy to acquire because of the very demanding underwater environment. First, the anchor-free scenarios commonly exist in the mid-depth ocean where AUVs hardly see anything but seawater. Some useful algorithms, such as SLAM [4], are not suitable. Second, anchor-free is an extremely harsh restriction that any involvement of device with known position will violate the assumptions. Thus, expectations of obtaining useful information from CNAs or using methods like opportunistic localization are not achievable. In this case, obtaining assistance from the ambient environments appears to be a viable option. Since the current exists throughout the ocean, we propose a current-aided localization algorithm that is adaptive in the SI.

Ocean general circulation models (OGCMs) [55] are a branch of the general circulation models to simulate the oceanic physical processes. These models have been developing fast and now can forecast the ocean current for several days with high resolution. Our current-aided localization algorithm fuses the measured current velocities with the predicted current map provided by OGCMs. The local current velocities can be measured by an acoustic Doppler current profiler, which is recently becoming standard for AUVs. The current map is generated by a certain kind of OGCM and preloaded on AUVs before deployment. The proposed method is named PCAF and composed of three steps: the position prediction, the map checking, and the weights update.

Algorithm 2: PCAF for AUV at Timestep t.

1: position prediction according to (29) and (30) and obtain $\boldsymbol{P}^{(t)}$
2: map checking according to (33) and obtain the "measured" position
3: update the weights of all particles in $\boldsymbol{P}^{(t)}$ according to (34)
4: normalize the updated weights
5: resample (with replacement) the weighted particles to obtain the output *belief* $\boldsymbol{B}^{(t)}$
6: compute the new position estimation $\hat{\boldsymbol{x}}_{i,\text{MMSE}}^{(t)}$ according to (28)

The position prediction operation is similar to that in UABP. In both UABP and PCAF, we use a set of weighted particles to represent the position distribution of an AUV. Thus, we still use the term *belief* to name the output particles of PCAF. Since each AUV navigates individually in the SI, we only consider a single-AUV self-localization problem in this section. Hence, the AUV index in the subscript is omitted. Suppose that the output *belief* from UABP at timestep $(t-1)$ is $\boldsymbol{B}^{(t-1)} = \{\mathbf{x}_{b,k}^{(t-1)}, w_{b,k}^{(t-1)}\}_{k=1}^{K}$ and the result of position prediction is $\boldsymbol{P}^{(t)} = \{\mathbf{x}_{pri,k}^{(t)}, w_{pri,k}^{(t)}\}_{k=1}^{K}$. The position prediction equations are as follows:

$$\mathbf{x}_{pri,k}^{(t)} = \mathbf{x}_{b,k}^{(t-1)} + v_k\tau\left[\sin(\theta_k);\, \cos(\theta_k)\right],$$
$$v_k \sim \mathcal{N}\left(\hat{v}^{(t-1)}, \sigma_v^{(t-1)2}\right),\quad \theta_k \sim \mathcal{N}\left(\hat{\theta}^{(t-1)}, \sigma_\theta^{(t-1)2}\right) \tag{29}$$

$$w_{pri,k}^{(t)} = w_{b,k}^{(t-1)} \tag{30}$$

where the definitions of $\hat{v}^{(t-1)}$, $\hat{\theta}^{(t-1)}$, $\sigma_v^{(t-1)}$, and $\sigma_\theta^{(t-1)}$ are the same as those in (15).

In the map checking, we compare the measured current velocities with the current map and convert the measurements into position information. We first define the map function as

$$\boldsymbol{v}_{c,\text{map}}^{(t)} = \boldsymbol{\Phi}(\boldsymbol{x}_{c,\text{map}}^{(t)}, t) + \boldsymbol{\zeta}_{c,\text{map}}^{(t)} \tag{31}$$

where $\boldsymbol{v}_{c,\text{map}}^{(t)}$ is the current velocity obtained from the map, $\boldsymbol{\Phi}$ and $\boldsymbol{x}_{c,\text{map}}^{(t)}$ denote the current map and corresponding coordinates, respectively, and $\boldsymbol{\zeta}_{c,\text{map}}^{(t)}$ indicates the prediction error of the map. Since the current velocities can be directly measured by sensors, we model the velocity observation as

$$\hat{\boldsymbol{v}}_c^{(t)} = \boldsymbol{v}_c^{(t)} + \boldsymbol{\delta}_c^{(t)} \tag{32}$$

where $\boldsymbol{v}_c^{(t)}$ is the real current velocity and $\boldsymbol{\delta}_c^{(t)}$ is the measurement noise. Our goal in map checking is to transform the current observation into position information. Thus, the "measured" position is given as

$$\hat{\boldsymbol{x}}_c^{(t)} = \arg\min_{x\in\mathcal{D}^{(t)}} \left\|\hat{\boldsymbol{v}}_c^{(t)} - \boldsymbol{v}_{c,\text{map}}^{(t)}\right\|_2 \tag{33}$$

Algorithm 3: IBPDR Framework.

```
AUVs i = 1 to N in parallel
    initialize the position variable x_i^(1) with coordinates of
    the known starting position
    initialize the belief uncertainty U_i^(n) = 1
end parallel
for t = 2 to Time do { time index }
    AUVs i to N in parallel
        estimate current position x^-_i^(t) with DR according
        to (13)
        if t ∈ T^C then
            correction operation by UABP with
            x̂_i^(t) = x̂_{i,MMSE}^(t): see Algorithm 1
        else
            no operation with x̂_i^(t) = x^-_i^(t) (or PCAF with
            x̂_i^(t) = x̂_{i,MMSE}^(t): see Algorithm 2)
        end if
    end parallel
end for
```

in which $\mathcal{D}^{(t)}$ is the local ambient region of the AUV, which is only a small part of the current map. Hence, no ambiguity of $\boldsymbol{v}_{c,\text{map}}^{(t)}$ would appear.

After obtaining the "measured" position information, we update the weights of all particles in $\boldsymbol{P}^{(t)}$ by

$$w_{b,k}^{(t)} \propto w_{pri,k}^{(t)} \exp\left\{-\frac{\left\|\mathbf{x}_{pri,k}^{(t)} - \hat{\boldsymbol{x}}_{c}^{(t)}\right\|_2^2}{2R_{\text{map}}}\right\} \quad (34)$$

where R_{map} indicates the resolution of the current map. Then, the weighted particles will go through the same normalization and resample operation, and the output *belief* at the timestep t is obtained as $\boldsymbol{B}^{(t)} = \{\mathbf{x}_{b,k}^{(t)}, w_{b,k}^{(t)}\}_{k=1}^{K}$. The procedure of PCAF is stated in **Algorithm 2**.

Now that we have introduced all the proposed methods, an overview of the proposed IBPDR framework is described in **Algorithm 3**.

E. Discussion

In this section, we deliver some guidances to illustrate how the proposed methods can be employed in real-world applications.

1) Since the proposed methods are based on the cooperation among AUVs, at least two underwater vehicles with inertial sensors, ranging, and communication equipments are required to adopt the methods.
2) The proposed methods focus on alleviating the impact of the accumulated inertial measurement errors. They should be applied after a period of navigation when the accumulated errors are relatively large, not from the beginning of the navigation. Since DR is able to provide high-accuracy position estimates in a short time, it is a suitable substitution for localization at the beginning.

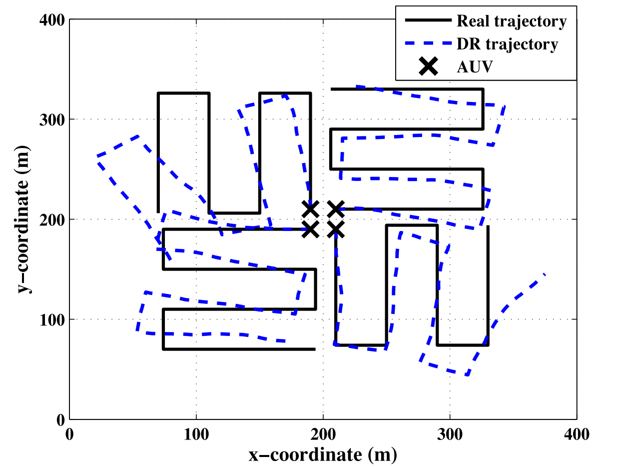

Fig. 3. Anchor-free scenarios: Four AUVs navigate in a plane without anchors.

3) The choices of the IBPDR period T and the angle uncertainty increment $\Delta\sigma_{\theta,i}$ are empirical and depend on the growth of the accumulated inertial measurement errors. With a low error growth (high-quality IMUs), the frequency of CL could be low. It indicates a relatively large T. On the other hand, $\Delta\sigma_{\theta,i}$ controls the growth of the accumulated uncertainty. When $\Delta\sigma_{\theta,i}$ is too small, Zone 2 cannot guarantee to cover the real position and effectively alleviate the impact of large accumulated errors. When $\Delta\sigma_{\theta,i}$ is large enough, Zone 2 can guarantee the coverage of the real position. Meanwhile, the distances among particles in Zone 2 will be large and the localization accuracy of the methods will degrade. Furthermore, the generation of the *message* in (21) requires the prior knowledge of the inter-AUV measurement uncertainties. When it is unknown, the obtained measurements can be used directly.
4) The current is not the only option that can be applied to assist localization in the SI. As a matter of fact, factors such as the geomagnetism, the gravity, the characteristics of seawater, etc., all can play the same role in the SI as long as the corresponding map is available. The qualities of the maps severely influence the localization accuracy and should be the key to determine which reference is chosen. When the maps are unavailable or with poor qualities, DR is still a choice in the SI.

V. Performance Evaluation

In this section, we evaluate our proposed algorithms by several numerical simulations. We consider a group of four AUVs navigating in 2-D planes, and each AUV carries all the necessary sensors and equipments for CL. Two typical scenarios, anchor-free and anchor-involved, are employed in the simulations. Although we focus on the anchor-free localization problems, we still would like to use the anchor-involved scenarios as counterparts to verify that our proposed methods can outperform others in not only anchor-free scenarios but also anchor-involved scenarios. Figs. 3 and 4 show the scenarios. In Fig. 3, a $400 \times 400\text{-m}^2$ anchor-free

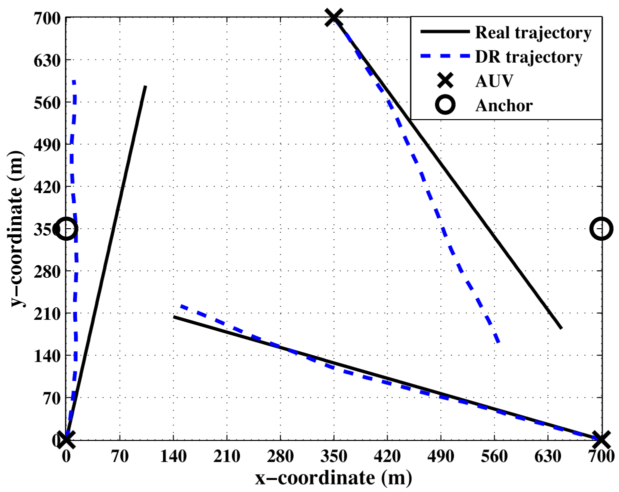

Fig. 4. Anchor-involved scenarios: Three AUVs navigate in a plane with two anchors.

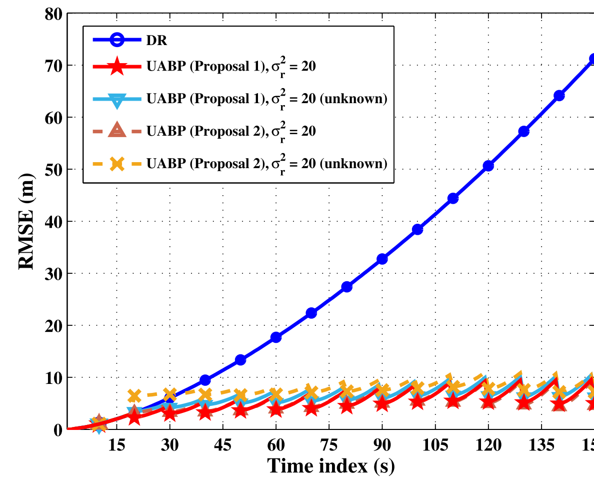

Fig. 5. Performance comparisons of different *proposals* in the anchor-involved scenario.

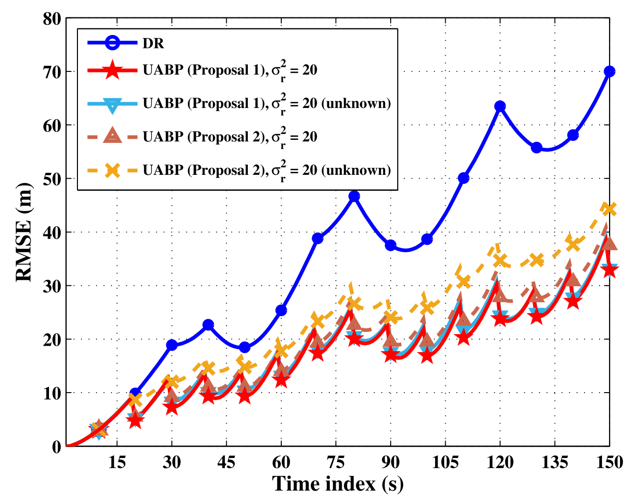

Fig. 6. Performance comparisons of different *proposals* in the anchor-free scenario.

plane is used. Lawn-mowing trajectories are designed for the AUVs. They are the typical paths for AUVs to scan a region in real applications. In addition, the trajectories contain several sharp turnings and may cause serious errors in the inertial measurements. As for the anchor-involved scenario, Fig. 4 shows a popular device deployment for CL including two anchors and three AUVs. It is applied in many relative works, such as in [21] and [25], to validate the designed BP-type algorithms. In both figures, cross and circle markers indicate AUVs and anchors, respectively, and the deviation of DR is clearly exhibited.

The evaluations consist of five parts. We first compare different choices of the *proposal* in UABP and find the best choice in our scenarios. Then, localization comparisons between the proposed algorithms and other popular ones are delivered. After that, we demonstrate the superiorities of the proposed IBPDR framework and PCAF method. Last but not least, some evaluations in packet loss, outliers, and ranging bias cases are discussed. All the simulations are based on the IBPDR framework with a period of 10 s (timesteps) and a total navigation time for 150 s. The first cooperation happens at the 20th second. The AUV speeds are set to 4 m/s. The measurements are corrupted by zero-mean Gaussian noises with variances for all AUVs, $\sigma_\theta^2 = 10$ or 1 (in anchor-free or anchor-involved scenarios, respectively), $\sigma_v^2 = 0.01$, $\sigma_r^2 = 20$, and $\sigma_b^2 = 25$ for heading angles, speeds, inter-AUV distances, and bearings, respectively. Note that the chosen parameters exaggerate the impact of the accumulated inertial measurement errors, resulting in DR's root-mean-square error (RMSE) reaching around 70 m after 150 s. The reasons are twofold. First, the proposed methods are designed to alleviate the impact of the accumulated errors and slow down DR's deviation, especially when the errors are large. A large deviation is more likely to testify the effectiveness of the proposed methods. Second, when DR's deviation is enlarged, different performance curves can be clearly separated. Hence, distinct comparisons among different methods or situations are exhibited in a short time navigation. The RMSE is calculated by averaging over all AUVs with 1000 Monte Carlo runs. The number of particles is 200. The choice of the particle number depends on the dimension of the problem and becomes a tradeoff. For a certain scenario, with more particles, a higher accuracy can be obtained while the requirements of computation and communication also grow higher. The angle uncertainty increment $\Delta\sigma_\theta$ is set to 0.5°. Note that the parameters in all examples are set according to the above statements. If there is any change of parameters, instructions will be stated.

A. *Choice of the Proposal*

As we have stated in Section IV-C, in UABP, the *message* multiplication can be roughly viewed as a sampling process from the *proposal*. Hence, the choice of the *proposal* needs sophisticated considerations. In the proposed algorithms, we select the *prior* (Proposal 1) as the *proposal* [23]. Another popular choice is to use the incoming *message* with the smallest entropy (Proposal 2) [20]. In AUV-localization, the "smallest entropy" *message* indicates the *message* transmitted from a neighboring AUV (or

TABLE II
ERROR CONDITIONS IN THE *Proposals*

Proposal	Different errors in the anchor-involved scenario		
	AUV/anchor position	inertial measurement	anchor-AUV measurement
Proposal 1	small	exist	none
Proposal 2	small	none	exist
	Different errors in the anchor-free scenario		
	AUV position	inertial measurement	inter-AUV measurement
Proposal 1	large	exist	none
Proposal 2	large	exist	exist

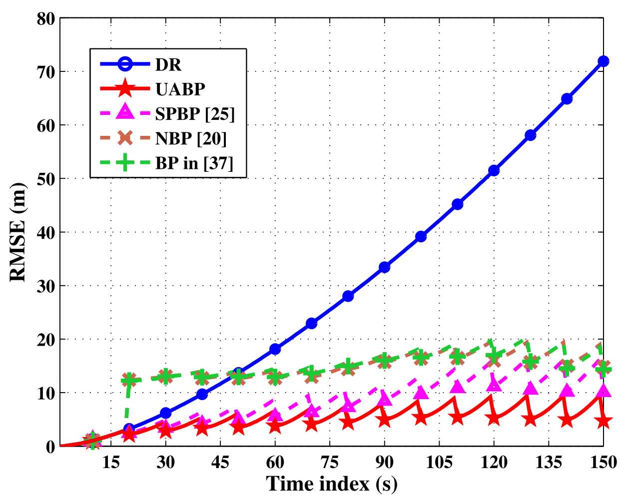

Fig. 7. Performance comparisons of different kinds of BP localization algorithms in the anchor-involved scenario.

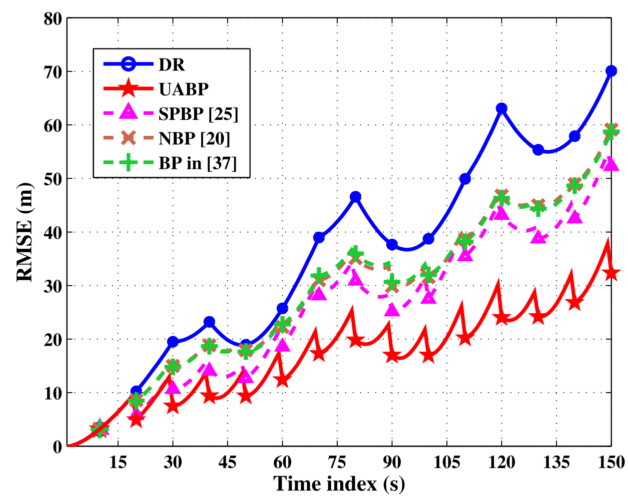

Fig. 8. Performance comparisons of different kinds of BP localization algorithms in the anchor-free scenario.

anchor) with the smallest position uncertainty. Figs. 5 and 6 show comparisons between these two kinds of *proposals*.

Both *proposals* provide position information of the AUV to be localized. Their effectiveness depends on the accuracy of the information. According to the definition of Proposal 1 (the *prior*) in Section IV-C, the error accumulation in obtaining Proposal 1 includes the position estimation errors at the last timestep and the inertial measurement errors. The error accumulation in Proposal 2 (the *message*) varies from different scenarios. It contains the position estimation errors of the neighboring AUVs, the inertial measurement errors, and the inter-AUV measurement errors in anchor-free scenarios. In anchor-involved scenarios, it contains the position uncertainty of the anchor and the anchor-AUV measurement errors. The error conditions in both *proposals* are exhibited in Table II.

In the anchor-involved scenario, the curves in Fig. 5 for Proposal 1 and Proposal 2 are overlapped. It is because that, with the help of the anchors, the errors in both *proposals* can be corrected. In this way, both *proposals* are able to provide accurate position information. However, in Fig. 6, more error sources are involved in Proposal 2 in the anchor-free scenario. Hence, the performance of Proposal 1 is better. Moreover, since Proposal 2 is the *message* transmitted from a neighboring AUV, its performance can be affected by the interaction conditions among AUVs. In both scenarios, the performance of Proposal 2 degrades when the prior knowledge of the inter-AUV measurement uncertainty is unknown and the measurements are used directly. In the meantime, since Proposal 1 is the *prior* obtained from the position prediction, its performance remains almost unchanged. Furthermore, the effectiveness of Proposal 2 can be severely corrupted by the communication conditions. In Section V-E, the good robustness of Proposal 1 to ill communication conditions is verified. Due to the above advantages of Proposal 1, we choose Proposal 1 as the *proposal* for UABP in our later simulations.

B. UABP Versus State of the Art

In underwater localization, the designed algorithms are expected to at least fulfill the following properties [2]: improved accuracy, low communication costs, fast convergence, and good scalability. In this section, we analyze the advantages of UABP according to these properties.

1) Localization Accuracy: In Figs. 7 and 8, the comparisons of RMSE among UABP and some state-of-the-art methods are exhibited. In the simulations, NBP [20] and BP applied in [37] are both particle-based methods. The choices of the *proposals* in them are on the basis of a principle that the chosen *proposals* give the best localization accuracy in the certain scenarios. SPBP [25] is another variant of the standard BP based on

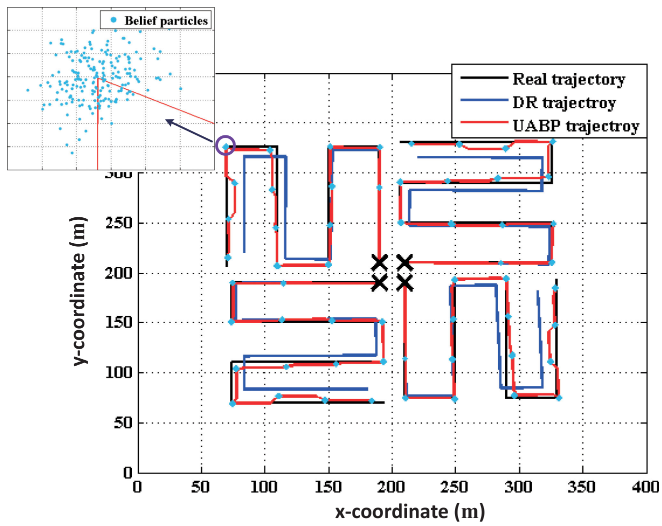

Fig. 9. Reconstructed trajectories in the anchor-free scenario.

TABLE III
AVERAGE BELIEF UNCERTAINTY

Time (s)	20	30	40	50	60	70	80
ABU (m^2)	8.94	20.01	26.47	31.27	30.53	26.79	31.94
Time (s)	90	100	110	120	130	140	150
ABU (m^2)	33.38	38.23	44.05	50.33	49.27	45.20	40.56

the unscented transform. The main advantage of SPBP for a distributed network is the low communication cost. From the results, we can see that, when the performance of DR continuously deteriorates, UABP always gives the best localization accuracy. It indicates the better resistance to the accumulated errors contained in the inertial measurements. The performance difference in the anchor-free scenario is more obvious than that in the anchor-involved scenario.

To better illustrate the localization performance, the reconstructed trajectories and the average *belief uncertainties* (ABUs) are presented in Fig. 9 and Table III, respectively. In Fig. 9, each AUV's reconstructed trajectory is obtained by averaging all its trajectories over 1000 Monte Carlo runs. Since each trajectory may diverge to different directions, the divergences of the trajectories alleviate with each other when they are averaged. This is why the localization errors in Fig. 9 are not as obvious as those in the RMSE figures or in a single Monte Carlo run (see Figs. 3 and 4). However, even in this case, the improvements in localization accuracy of UABP are obvious. The blue dots on the red curves are the output particles of the *belief*. Since the MMSE position estimates are obtained by calculating the means of these particles, the *belief uncertainties* indicate the estimation uncertainties based on these *belief* particles. In Table III, the ABUs are calculated by averaging the *belief uncertainties* over all AUVs with 1000 Monte Carlo runs.

2) Communication Costs: In distributed networks, reducing the communication costs is very important, and even more underwater. Table IV gives the number of real numbers need to be transmitted from a single AUV in a single cooperation. In

TABLE IV
NUMBER OF TRANSMITTED REAL NUMBERS FROM ONE AUV IN ONE COOPERATION

Algorithm	Number of transmitted numbers	
	In theory	In our simulation
NBP [20]	$K \times \eta$	400
BP in [37]	$K \times \eta$	400
SPBP [25]	$\eta^2 + \eta$	6
UABP	$\eta + 1$	3

the table, K is the number of particles used in the particle-based methods, η is the dimension of the position variable $\boldsymbol{x}_i^{(t)}$. Usually, an AUV transmits all the particles as the representation of its *belief* to neighbors. The transmitted data volume is huge. SPBP has decreased the data volume to a mean vector and a covariance matrix, which are composed of $\eta + \eta^2$ real numbers. However, a primary restriction of SPBP worth mentioning is that SPBP is limited to the Gaussian measurement model [26], which is not in line with underwater localization issues. UABP has further approximated the data to a mean vector and an uncertainty parameter, which require $\eta + 1$ real numbers.

The average runtimes of the 1000 Monte Carlo runs for UABP, BP in [37], NBP, and SPBP in the anchor-free scenario are 0.205, 0.177, 0.175, and 0.040 s, respectively. They are measured by MATLAB with an Intel i7-7700HQ CPU. From the results, UABP has the longest runtime. It is because generating angle particles in (15) costs extra time. Since the energy consumption for transmitting one bit of information can support the execution of thousands of instructions [30], we believe that the small extra computational costs will not affect the feasibility of UABP.

3) Convergence: The UABP is a modification of BP according to the underwater scenarios. It inherits the basic structure and principles of BP. Thus, the theoretical convergence of UABP is guaranteed and remains the same as that of the standard BP as stated in Section III, [22], and [29]. The iterations for convergence are smaller than the length of the longest path in the graph defined in Section III. During localization, since each AUV has its own prior position information and only communicates with its neighbors, only one iteration of UABP is needed to perform localization. Comparisons of UABP with different iterations are exhibited in Fig. 10. The tiny differences among the curves indicate that there is no necessity to increase the iterations. Because each iteration requires communications among all AUVs, hence we limit the iteration number to one.

In this way, the communication costs are further reduced, and the overconfidence problem in the multi-iteration BP applications is prevented [50]. Note that, in this article, we implement UABP in anchor-free environments. Although UABP converges and provides position estimates at each timestep, the localization errors of the whole AUV navigation still grow without bound. It is because the inertial measurement errors are accumulative and grow unbounded. No matter what algorithm is applied, the error growth can be bounded only with the help of the absolute references (anchors).

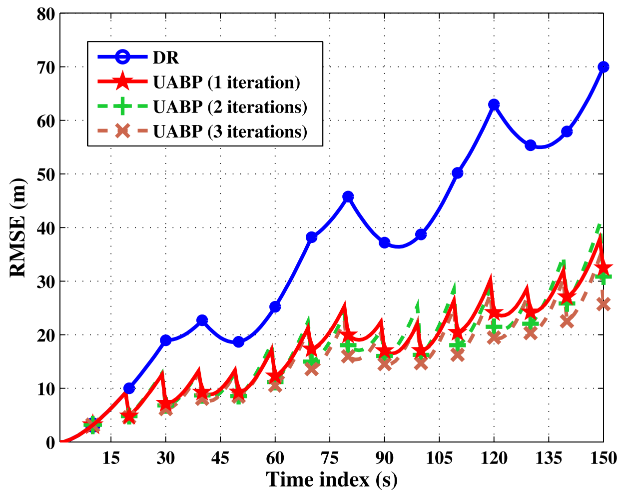

Fig. 10. Performance comparisons of UABP with different iterations.

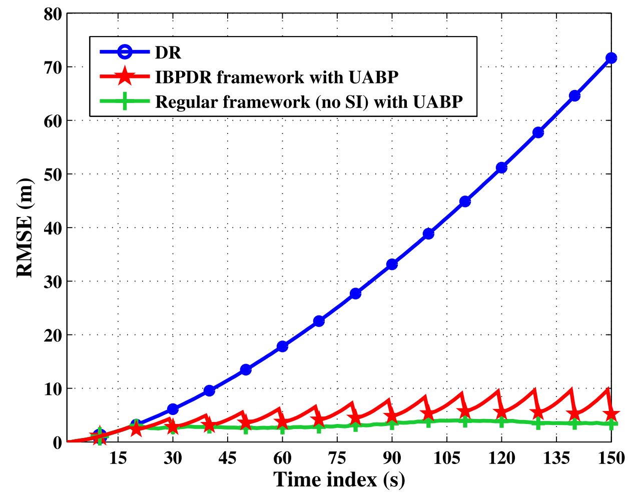

Fig. 11. Performance comparisons between the IBPDR framework and the regular framework in the anchor-involved scenario.

4) Scalability: Since BP is a naturally distributed algorithm, AUVs only need to communicate with their neighbors to perform localization. Moreover, BP is based on the graphical models and operates in both time and space. It is less computationally complex (grows linearly to the network size) since the joint PDF can be factorized over the graph. Thus, the good scalability is one of BP's strengths. It enables the application of BP in large networks. The proposed UABP is a particle-based extension of BP. It inherits the basic structure of BP. Hence, the advantages of BP are retained in UABP. Meyer *et al.* [23] have testified the scalability of the particle-based BP, making comparisons among the particle-based BP, the sampling importance resampling particle filter, and the unscented particle filter. The results show that the particle-based BP has better scalability that its computational amount is linear to the network size. Moreover, in UABP, the limitation of iteration and the reduction of communication costs further lower the requirements among AUVs when the team grows larger.

In summary, UABP outperforms the state-of-the-art methods in localization accuracy and communication costs, while it inherits the advantages of BP in convergence and scalability aspects.

C. IBPDR Versus the Regular Framework Without the SI

In this section, we would like to validate the advantages of the proposed IBPDR framework. An important feature of IBPDR is the existence of the SI. If there is no SI, the framework is referred to as the regular framework where cooperation happens at every timestep. We now exhibit comparisons between two frameworks.

Figs. 11 and 12 show the RMSE results. In the anchor-involved scenario, the regular framework has a better performance. This corresponds with the common sense that a higher frequency of communications with anchors gives a better localization accuracy. However, in the anchor-free scenario, two performance curves are almost overlapped.

To clearly show the differences, a quantitative analysis of the RMSE at the correction timesteps is established in Table V. We also draw another curve with the RMSE of IBPDR at the correction timesteps, the yellow-dotted curve in Fig. 12. From the results, the RMSE of the IBPDR framework at the correction timesteps is always smaller than that of the regular framework. By localization with anchors, the localization errors can be easily corrected or maintained within certain accuracy. However, in anchor-free scenarios, decent corrections are difficult to accomplish, and the error growth is unbounded. Taking the curves in an IBPDR period (between two consecutive markers)

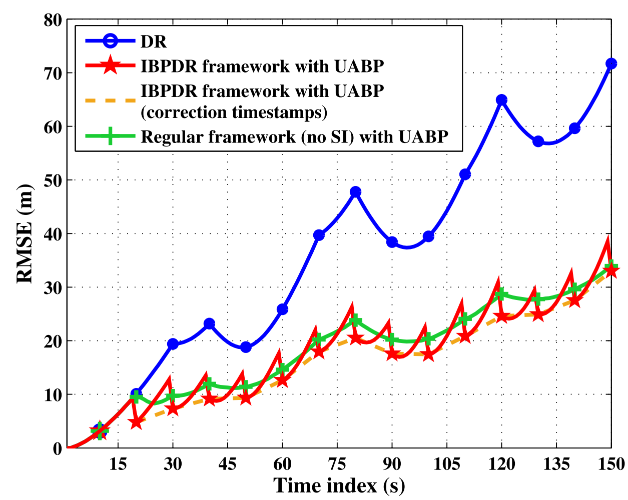

Fig. 12. Performance comparisons between the IBPDR framework and the regular framework in the anchor-free scenario.

TABLE V
RMSE of Different Frameworks at the Correction Timesteps

Framework	RMSE (m) at the correction timesteps							
	Time (s)	20	30	40	50	60	70	80
IBPDR		4.78	7.34	9.15	9.33	12.63	17.95	20.52
Regualr		9.52	9.74	11.94	11.40	14.59	20.24	23.84
	Time (s)	90	100	110	120	130	140	150
IBPDR		17.25	17.45	20.87	24.59	24.91	27.53	33.00
Regualr		20.21	20.36	24.06	28.72	27.77	29.60	33.95

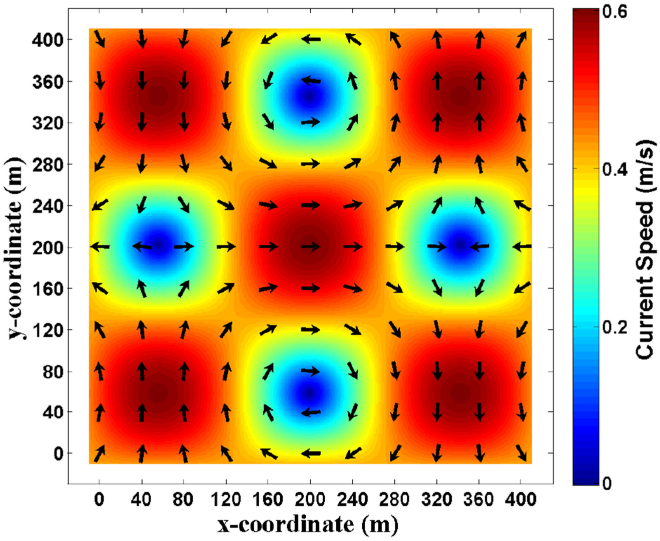

Fig. 13. Current field with the maximum current speed equals to 0.6 m/s

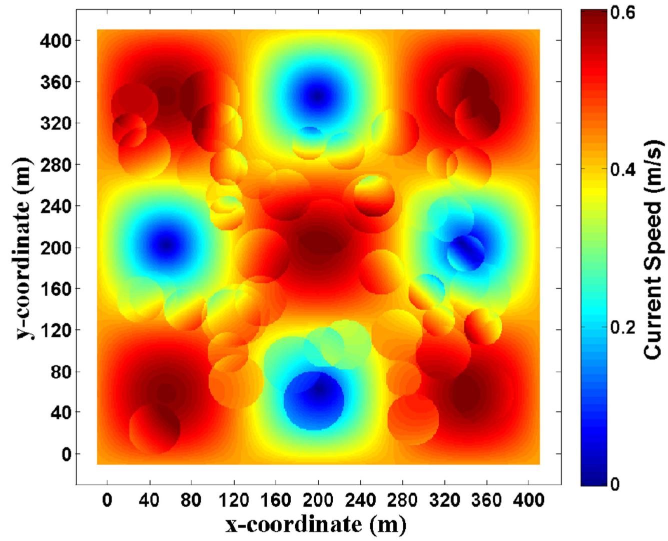

Fig. 14. Current field affected by turbulence.

in Fig. 12 as an example, the green curve (the regular framework) grows mildly while the red one (the IBPDR framework) grows very fast. It indicates that applying CL among AUVs at every timestep indeed helps to slow down the growth of the localization error. However, when we compare the localization accuracy at the correction timesteps, the IBPDR framework performs better. It is because more cooperative estimation errors are accumulated at each cooperation, especially when the accuracy of the inter-AUV measurements is not high in underwater fields. High-frequency cooperations accelerate the accumulation of the cooperative estimation errors. Moreover, according to (17), the inertial measurement errors accumulated during the current IBPDR period can be further alleviated by an average operation. These are the main reasons why IBPDR has better localization accuracy in anchor-free environments. Furthermore, the cooperative communication costs are reduced in IBPDR. Assuming that the total communication costs in the regular framework for a single IBPDR period are E, the communication costs reduce to E/n in IBPDR (n is the number of time slots in an IBPDR period). Thus, in both localization accuracy and communication cost aspects, the proposed IBPDR framework is more suitable for the anchor-free scenarios.

D. DR Versus PCAF in the SI

In this section, we will focus on the performance evaluation about the noncooperative methods used in the SI. The main reason for introducing the new noncooperative methods is that we would like to bring in more useful information to assist localization without increasing the communication costs. Fig. 13 shows the basic current field [41] that we apply in the simulation. Its range covers the navigation region of all AUVs. In reality, the current speed varies from 0.08 to 2.5 m/s [56]. Our choice of the current speed is based on the current charts of the South China Sea in [57], where the speed varies within 1.2 kn (approximately equals to 0.6 m/s). Thus, in this simulation, the current speed varies from 0 to 0.6 m/s.

However, the predicted current map usually cannot perfectly match the real current condition in practice. To make the simulation more convincing, we add vortices as current turbulence in the scenario. The predicted current map is not aware of the existence of these vortices. The vortices are modeled as [58]

$$V_x(\boldsymbol{x}) = -\Gamma\frac{\beta-\beta_c}{2\pi(\boldsymbol{x}-\boldsymbol{x}_c)^2}\left\{1-\exp\left[\frac{(\boldsymbol{x}-\boldsymbol{x}_c)^2}{r^2}\right]\right\} \quad (35)$$

$$V_y(\boldsymbol{x}) = \Gamma\frac{\alpha-\alpha_c}{2\pi(\boldsymbol{x}-\boldsymbol{x}_c)^2}\left\{1-\exp\left[\frac{(\boldsymbol{x}-\boldsymbol{x}_c)^2}{r^2}\right]\right\} \quad (36)$$

where $V_x(\boldsymbol{x})$ ($V_y(\boldsymbol{x})$) is the vortex speed along the x-axis (y-axis), $\boldsymbol{x} = [\alpha, \beta]^T$ is the position variable, $\boldsymbol{x}_c = [\alpha_c, \beta_c]^T$ indicates the coordinates of the vortex center, Γ denotes the strength of the vortex, and r represents the radius of the vortex. Fig. 14 shows the current field affected by 50 vortices. All the vortices are randomly distributed in the current field, with $\Gamma \sim \mathcal{U}(6, 63)$ and $r \sim \mathcal{U}(15, 30)$. It results that the maximum speed of each vortex varies from 0.01 to 0.2 m/s.

The different performances are demonstrated in Fig. 15, in which comparisons between UABP with no aid and UABP aided by PCAF with (or without) perfectly predicted current map are elaborated. We can see that the use of current information makes clear improvements in localization. However, the efficiency of the algorithm depends on how useful the information can be. In fact, the accuracy of the map has large impact on the effectiveness of the algorithm. This is why we cannot only apply PCAF for localization but under the IBPDR framework. In this way, even if the prediction accuracy is bad, IBPDR will still give a reasonable result, which is guaranteed by the cooperative algorithms.

E. Packet Loss, Ranging Bias, and Outlier

Last but not least, we discuss the influences about packet loss, ranging bias, and outliers. In CL, communications among devices are indispensable. However, the underwater communication environment is very challenging. Thus, packet loss

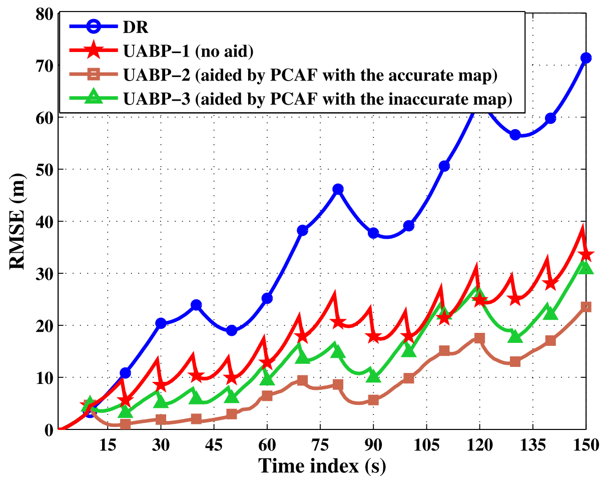

Fig. 15. Performance comparisons between UABP with or without assistance by PCAF in the anchor-free scenario. UABP-1 is not aided by the current. UABP-2 uses the current map perfectly matching the current field, and UABP-3 uses the current map not aware of the turbulence in the current field.

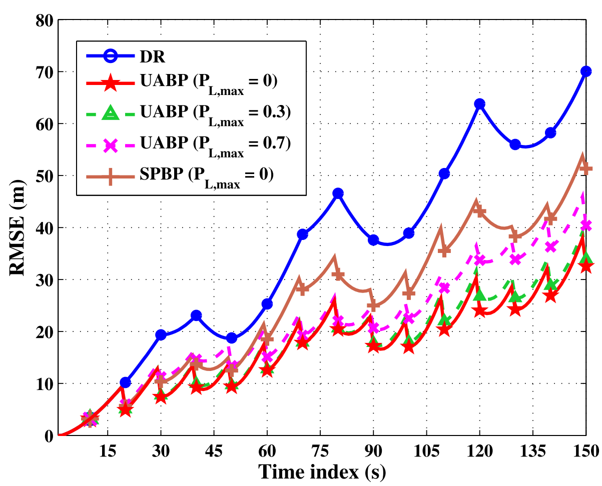

Fig. 16. Performance comparisons of packet-loss cases between UABP and SPBP with different packet-loss probabilities in the anchor-free scenario.

ranging bias and outliers often happen. Fig. 16 shows the RMSE results of packet-loss cases, where $P_{L,\max}$ indicates the maximum packet-loss probability. We have compared the performance among UABP with different $P_{L,\max}$. In addition, since SPBP outperforms NBP and BP in [37], we also add SPBP in the comparison to show the superiorities of UABP. In our simulations, the model of the successful communication probability proposed in [59] is used

$$P_s(\boldsymbol{x}_i^{(t)}, \boldsymbol{x}_j^{(t)}) = \exp\left(-\frac{\left\|\boldsymbol{x}_i^{(t)} - \boldsymbol{x}_j^{(t)}\right\|^2}{2R^2}\right) \tag{37}$$

where P_s indicates the successful communication probability between the ith and jth AUVs, R is a constant. Thus, the packet-loss probability P_L is defined as $P_L(\boldsymbol{x}_i^{(t)}, \boldsymbol{x}_j^{(t)}) = 1 - P_s(\boldsymbol{x}_i^{(t)}, \boldsymbol{x}_j^{(t)})$. $P_{L,\max}$ is the packet-loss probability when the distance between two AUVs reaches the farthest. For example, $P_{L,\max} = 0.3$ indicates that, within 1000 Monte Carlo runs,

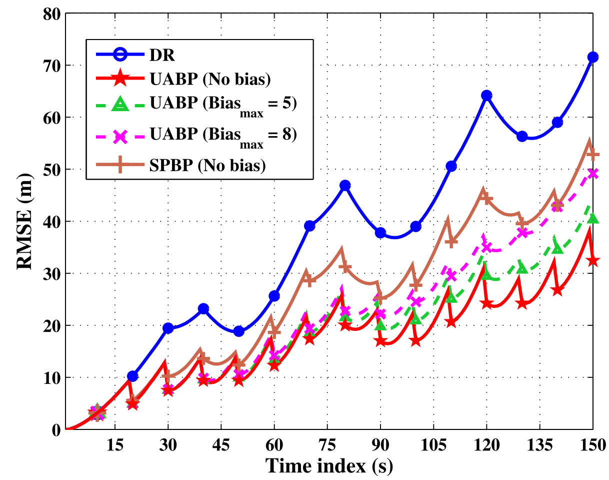

Fig. 17. Performance comparisons between UABP and SPBP with different ranging biases in the anchor-free scenario.

about 300 runs suffer packet loss when two AUVs reach the farthest distance.

Fig. 16 validates UABP's robustness in packet-loss cases. When $P_{L,\max}$ equals to 0.3, the accuracy loss of UABP is little. Furthermore, when $P_{L,\max}$ reaches 0.7, the localization accuracy of UABP is still higher than that of SPBP with no packet loss.

More than the missing data cases, the bias in the range measurement is also a common factor of accuracy degradation. A ranging bias is usually caused by asynchronization between devices. In the simulation, we simply add ranging biases that grow linearly over time, $\text{Bias} = at + b$, with the maximum bias $\text{Bias}_{\max}$ reaches around 5 ($a \sim \mathcal{N}(0.025, 0.001^2)$, $b \sim \mathcal{N}(1, 0.05^2)$) and 8 ($a \sim \mathcal{N}(0.045, 0.001^2)$, $b \sim \mathcal{N}(1, 0.05^2)$) at the end of the navigation. Fig. 17 shows the superiorities of UABP in ranging bias cases.

Note that both packet loss and ranging bias only affect the usabilities of the transmitted *messages*. In UABP, to obtain a good position estimate, we only need to filter the particles near the real position (see Zone 4 in Fig. 2) out of the *prior* by the received *messages*. As long as the *prior* covers the true position, useful *messages* give the particles near the true position high weights (see more details in Section IV). Since the generation of the *prior* is by the position prediction, it is not influenced by the communication conditions. In such circumstances, even with only one relatively accurate *message*, the accuracy of the position estimate can be guaranteed. For example, in our scenarios, each AUV has three neighbors. As long as one relatively accurate *message* is obtained by the AUV, its position estimate would not degrade greatly even if the packet loss or ranging bias happens. This is why UABP has good robustness in both cases.

At last, we discuss the outliers. In the range-based CL, outliers usually happen in the ranging process. The outlier cases are usually considered in large-scale wireless networks to which our scenario can easily extend. In UABP, the range measurements are used to generate the *messages* and then calculate the weights of the particles from the *proposal* according to (27). When an outlier appears and generates a wrong *message* $\hat{m}_{\text{wrong}}$, the distances between particles from $\hat{m}_{\text{wrong}}$ and the *proposal* would be large. Since we use KDE with Gaussian kernels to approximate the *messages*, the output value of *message* $\hat{m}_{\text{wrong}}(\mathbf{x}_{p,k,i}^{(t)})$ in (27) would be extremely small. Thus, by setting a threshold of the *messages'* output values in (27), the outlier cases can be converted to the packet-loss cases in which the superiorities of UABP have already been proved.

VI. Conclusion

The problem of multi-AUV CL in anchor-free environments is investigated in this article. In anchor-free environments, with only relative inter-AUV measurements and drifted inertial measurements, the growth of localization errors cannot be bounded. This work is devoted to slow down the growth of the localization errors by means of cooperations among AUVs. Due to communications in cooperations and energy limitations in underwater applications, reducing the communication costs among AUVs is also considered.

The main contributions of this article are as follows. First, we designed an intermittent CL framework named IBPDR. In IBPDR, AUVs cooperatively localize themselves once a period using the proposed UABP algorithm, and each AUV uses the proposed PCAF algorithm for self-localization when no cooperation happens. In this way, the communication costs are reduced by decreasing the number of communications, and the overall localization accuracy is improved by cooperations among AUVs. Moreover, IBPDR provides a combination of cooperative and noncooperative methods. Second, we proposed a particle-based fully distributed CL method named UABP. The position prediction process in UABP considers the accumulated inertial measurement errors and alleviates their impact. We also use parametric approximations to reduce the communication costs. In addition, the use of the particles makes UABP feasible in nonlinear and non-Gaussian scenarios. The distributed fashion of UABP provides a good scalability when it is applied in large networks. Finally, we design a PCAF, in which localization is achieved by checking the measured ambient current in the predicted current map. PCAF brings in useful current information to assist localization without increasing the communication costs. However, the efficiency of PCAF relies on the quality of the current map.

Simulation results demonstrate that the proposed methods outperform the state-of-the-art methods in the localization accuracy, communication cost, robustness to bad cases, etc. Since the positions are the basic information for multi-AUV applications, based on this work, the future work can focus on accomplishing certain tasks, such as tracking noncooperative targets, and multi-AUV path planning and following.

References

[1] R. B. Wynn *et al.*, "Autonomous underwater vehicles (AUVs): Their past, present and future contributions to the advancement of marine geoscience," *Mar. Geol.*, vol. 352, pp. 451–468, Jun. 2014.

[2] H. Tan, R. Diamant, W. K. G. Seah, and M. Waldmeyer, "A survey of techniques and challenges in underwater localization," *Ocean Eng.*, vol. 38, no. 14, pp. 1663–1676, Oct. 2011.

[3] M. Chitre, S. Shahabudeen, and M. Stojanovic, "Underwater acoustic communications and networking: Recent advances and future challenges," *Mar. Technol. Soc. J.*, vol. 42, no. 1, pp. 103–116, 2008.

[4] L. Paull, S. Saeedi, M. Seto, and H. Li, "AUV navigation and localization: A review," *IEEE J. Ocean. Eng.*, vol. 39, no. 1, pp. 131–149, Jan. 2014.

[5] J. Melo and A. Matos, "Survey on advances on terrain based navigation for autonomous underwater vehicles," *Ocean Eng.*, vol. 139, pp. 250–264, May 2017.

[6] G. Tuna and V. C. Gungor, "A survey on deployment techniques, localization algorithms, and research challenges for underwater acoustic sensor networks," *Int. J. Commun. Syst.*, vol. 30, no. 17, Jun. 2017.

[7] S. I. Roumeliotis and G. A. Bekey, "Distributed multirobot localization," *IEEE Trans. Robot. Autom.*, vol. 18, no. 5, pp. 781–795, Oct. 2002.

[8] Y. Shen, H. Wymeersch, and M. Z. Win, "Fundamental limits of wideband localization—Part II: Cooperative networks," *IEEE Trans. Inf. Theory*, vol. 56, no. 10, pp. 4981–5000, Oct. 2010.

[9] M. Chitre, "Teamwork among AUVs," in *Proc. AUV Sensors Syst. Workshop*, Kona, HI, USA, Nov. 2010.

[10] M. Chitre, "Teamwork among marine robots–advances and challenges," in *Proc. Workshop Mar. Robot.*, Las Palmas de Gran Canaria, Spain, Feb. 2013.

[11] N. Patwari, J. N. Ash, S. Kyperountas, A. O. Hero, R. L. Moses, and N. S. Correal, "Locating the nodes: Cooperative localization in wireless sensor networks," *IEEE Signal Process. Mag.*, vol. 22, no. 4, pp. 54–69, Jul. 2005.

[12] M. Z. Win *et al.*, "Network localization and navigation via cooperation," *IEEE Commun. Mag.*, vol. 49, no. 5, pp. 56–62, May 2011.

[13] B. Denis, J.-B. Pierrot, and C. Abou-Rjeily, "Joint distributed synchronization and positioning in UWB ad hoc networks using TOA," *IEEE Trans. Microw. Theory Techn.*, vol. 54, no. 4, pp. 1896–1911, Jun. 2006.

[14] N. Trawny, S. I. Roumeliotis, and G. B. Giannakis, "Cooperative multi-robot localization under communication constraints," in *Proc. IEEE Int. Conf. Robot. Autom.*, May 2009, pp. 4394–4400.

[15] A. Howard, M. J. Mataric, and G. S. Sukhatme, "Putting the 'I' in 'team': An ego-centric approach to cooperative localization," in *Proc. IEEE Int. Conf. Robot. Autom.*, Taipei, Taiwan, Sep. 2003, pp. 868–874.

[16] A. Bahr, M. R. Walter, and J. J. Leonard, "Consistent cooperative localization," in *Proc. IEEE Int. Conf. Robot. Autom.*, Kobe, Japan, May 2009, pp. 3415–3422.

[17] G. Rui and M. Chitre, "Cooperative positioning using range-only measurements between two AUVs," in *Proc. IEEE OCEANS Conf.*, Sydney, Australia, May 2010, pp. 1–6.

[18] G. P. Huang, N. Trawny, A. I. Mourikis, and S. I. Roumeliotis, "Observability-based consistent EKF estimators for multi-robot cooperative localization," *Auton. Robots*, vol. 30, no. 1, pp. 99–122, Jan. 2011.

[19] J. Pearl, *Probabilistic Reasoning in Intelligent Systems: Networks of Plausible Inference*. San Mateo, CA, USA: Morgan Kaufmann, 1988.

[20] J. Lien, U. J. Ferner, W. Srichavengsup, H. Wymeersch, and M. Z. Win, "A comparison of parametric and sample-based message representation in cooperative localization," *Int. J. Navigat. Observ.*, vol. 2012, pp. 1–10, Jul. 2012.

[21] H. Wymeersch, J. Lien, and M. Z. Win, "Cooperative localization in wireless networks," *Proc. IEEE*, vol. 97, no. 2, pp. 427–450, Feb. 2009.

[22] B. Etzlinger, F. Meyer, F. Hlawatsch, A. Springer, and H. Wymeersch, "Cooperative simultaneous localization and synchronization in mobile agent networks," *IEEE Trans. Signal Process.*, vol. 65, no. 14, pp. 3587–3602, Jul. 2017.

[23] F. Meyer, O. Hlinka, H. Wymeersch, E. Riegler, and F. Hlawatsch, "Distributed localization and tracking of mobile networks including noncooperative objects," *IEEE Trans. Signal Inf. Process. Netw.*, vol. 2, no. 1, pp. 57–71, Mar. 2016.

[24] Á. F. García-Fernández, L. Svensson, and S. Särkkä, "Cooperative localization using posterior linearization belief propagation," *IEEE Trans. Veh. Technol.*, vol. 67, no. 1, pp. 832–836, Jan. 2018.

[25] F. Meyer, O. Hlinka, and F. Hlawatsch, "Sigma point belief propagation," *IEEE Signal Process. Lett.*, vol. 21, no. 2, pp. 145–149, Feb. 2014.

[26] H. M. Georges, Z. Xiao, and D. Wang, "Hybrid cooperative vehicle positioning using distributed randomized sigma point belief propagation on non-Gaussian noise distribution," *IEEE Sensors J.*, vol. 16, no. 21, pp. 7803–7813, Nov. 2016.

[27] S. Li, M. Hedley, and I. B. Collings, "New efficient indoor cooperative localization algorithm with empirical ranging error model," *IEEE J. Sel. Areas Commun.*, vol. 33, no. 7, pp. 1407–1417, Jul. 2015.

[28] A. T. Ihler, J. W. Fisher, R. L. Moses, and A. S. Willsky, "Nonparametric belief propagation for self-localization of sensor networks," *IEEE J. Sel. Areas Commun.*, vol. 23, no. 4, pp. 809–819, Apr. 2005.

[29] V. Savic and S. Zazo, "Cooperative localization in mobile networks using nonparametric variants of belief propagation," *Ad Hoc Netw.*, vol. 11, no. 1, pp. 138–150, May 2013.

[30] V. Savic and S. Zazo, "Reducing communication overhead for cooperative localization using nonparametric belief propagation," *IEEE Wireless Commun. Lett.*, vol. 1, no. 4, pp. 308–311, Aug. 2012.

[31] Y. Huang, W. Liang, H. Yu, and Y. Xiao, “Target tracking based on a distributed particle filter in underwater sensor networks,” *Wireless Commun. Mobile Comput.*, vol. 8, no. 8, pp. 1023–1033, 2008.
[32] M. Chitre, “Path planning for cooperative underwater range-only navigation using a single beacon,” in *Proc. Int. Conf. Auton. Intell. Syst.*, Povoa de Varzim, Portugal, Jun. 2010, pp. 1–6.
[33] D. B. Edwards, T. A. Bean, D. L. Odell, and M. J. Anderson, “A leader-follower algorithm for multiple AUV formations,” in *Proc. IEEE/OES Auton. Underwater Veh. Conf.*, Sebasco Estates, ME, USA, Jun. 2004, pp. 40–46.
[34] W. Xing, Y. Zhao, and H. R. Karimi, “Convergence analysis on multi-AUV systems with leader-follower architecture,” *IEEE Access*, vol. 5, pp. 853–868, 2017.
[35] M. F. Fallon, G. Papadopoulos, J. J. Leonard, and N. M. Patrikalakis, “Cooperative AUV navigation using a single maneuvering surface craft,” *Int. J. Robot. Res.*, vol. 29, no. 12, pp. 1461–1474, Aug. 2010.
[36] A. Bahr, J. J. Leonard, and M. F. Fallon, “Cooperative localization for autonomous underwater vehicles,” *Int. J. Robot. Res.*, vol. 28, no. 6, pp. 714–728, Jun. 2009.
[37] Y. Li, Y. Wang, and X. Guan, “Belief propagation based multi-AUV cooperative localization in anchor-free environments,” in *Proc. 4th Underwater Commun. Netw. Conf.*, Lerici, Italy, Aug. 2018, pp. 1–5.
[38] T. Pan and T. Hou, “Localization of moving nodes in an anchor-less wireless sensor network,” in *Proc. IEEE Wireless Commun. Netw. Conf.*, Shanghai, China, Apr. 2012, pp. 3112–3116.
[39] Y. Xie, J. Liu, C. Hu, J. Cui, and H. Xu, “AUV dead-reckoning navigation based on neural network using a single accelerometer,” in *Proc. 11th ACM Int. Conf. Underwater Netw. Syst.*, Shanghai, China, Oct. 2016, pp. 1–5.
[40] G. Salavasidis *et al.*, “Terrain-aided navigation for long-endurance and deep-rated autonomous underwater vehicles,” *J. Field Robot.*, vol. 36, no. 2, pp. 447–474, 2019.
[41] Z. Song and K. Mohseni, “Cooperative mid-depth navigation aided by ocean current prediction,” in *Proc. OCEANS*, Anchorage, AK, USA, Sep. 2017, pp. 1–8.
[42] Y. Guo and Y. Liu, “Localization for anchor-free underwater sensor networks,” *Comput. Elect. Eng.*, vol. 39, no. 6, pp. 1812–1821, Aug. 2013.
[43] A. Kukulya *et al.*, “Under-ice operations with a REMUS-100 AUV in the Arctic,” in *Proc. IEEE/OES Auton. Underwater Veh.*, Monterey, CA, USA, Sep. 2010, pp. 1–8.
[44] O. J. Woodman, “An introduction to inertial navigation,” , Comput. Lab., Univ. Cambridge, Cambridge, U.K., Tech. Rep. UCAMCL-TR-696, 2007.
[45] J. S. Yedidia, W. T. Freeman, and Y. Weiss, “Understanding belief propagation and its generalizations,” in *Exploring Artificial Intelligence in the New Millennium*, San Francisco, CA, USA: Morgan Kaufmann, 2003, pp. 236–239.
[46] D. Koller, N. Friedman, and F. Bach, *Probabilistic Graphical Models: Principles and Techniques*. Cambridge, MA, USA: MIT Press, 2009.
[47] S. L. Lauritzen, *Graphical Models*. London, U.K.: Oxford Univ. Press, 1996.
[48] J. Besag, “Spatial interaction and the statistical analysis of lattice systems,” *J. Roy. Statist. Soc. B, Methodol.*, vol. 36, no. 2, pp. 192–236, 1974.
[49] J. Liu, Z. Wang, J.-H. Cui, S. Zhou, and B. Yang, “A joint time synchronization and localization design for mobile underwater sensor networks,” *IEEE Trans. Mobile Comput.*, vol. 15, no. 3, pp. 530–543, Mar. 2016.
[50] M. Frhle and H. Wymeersch, “On the separation of timescales in radio-based positioning,” in *Proc. ICL-GNSS*, Gothenburg, Sweden, Jun. 2015, pp. 1–6.
[51] B. W. Silverman, *Density Estimation For Statistics and Data Analysis*. New York, NY, USA: Chapman & Hall, 1986.
[52] A. T. Ihler, *“Inference in Sensor Networks: Graphical Models and Particle Methods,”* Ph.D. dissertation, Massachusetts Inst. Technol., Cambridge, MA, USA, 2005.
[53] A. Doucet, N. De Freitas, and N. Gordon, *Sequential Monte Carlo Methods in Practice*. New York, NY, USA: Springer, 2001.
[54] M. S. Arulampalam, S. Maskell, N. Gordon, and T. Clapp, “A tutorial on particle filters for online nonlinear/non-Gaussian Bayesian tracking,” *IEEE Trans. Signal Process.*, vol. 50, no. 2, pp. 174–188, Feb. 2002.
[55] A. Mehra and I. Rivin, “A real time ocean forecast system for the North Atlantic Ocean,” *Terrestrial Atmos. Ocean. Sci.*, vol. 21, no. 1, pp. 211–228, Feb. 2010.
[56] M. G. Gross, *Oceanography: A View of the Earth.* 3rd ed. New York, NY, USA: Prentice-Hall, 1982.
[57] J. Hu, H. Kawamura, H. Hong, and Y. Qi, “A review on the currents in the South China Sea: Seasonal circulation, South China Sea warm current and Kuroshio intrusion,” *J. Oceanography*, vol. 56, no. 6, pp. 607–624, 2000.
[58] H. Lamb, *Hydrodynamics*. Cambridge, U.K.: Cambridge Univ. Press, 1993.
[59] R. L. Moses and R. Patterson, “Self-calibration of sensor networks,” *Proc. SPIE*, vol. 4743, pp. 108–120, 2002.

Yichen Li (S’18) received the B.S. degree in electronics and information from Northwestern Polytechnical University, Xi’an, China, in 2016. He is currently working toward the Ph.D. degree at the Department of Automation, School of Electronic Information and Electrical Engineering, Shanghai Jiao Tong University, Shanghai, China.

His current research interests include mobile-robot localization, wireless networks, and information fusion.

Yiyin Wang (M’11) received the B.S. degree in electrical engineering from Fudan University, Shanghai, China, in 2002, the M.S. degree (*cum laude*) in microelectronics from the Delft University of Technology (TU Delft), Delft, The Netherlands, and Fudan University, Shanghai, China, in 2005, respectively, and the Ph.D. degree in electrical engineering from TU Delft, in 2011.

She was a Research Assistant with the Circuits and Systems Group, TU Delft, from 2006 to 2007. In 2010, she visited the Georgia Institute of Technology (Gatech), Atlanta, GA, USA. She was a Postdoctoral Fellow with TU Delft and then Gatech from 2011 to 2013. She is currently an Associate Professor with the Department of Automation, Shanghai Jiao Tong University, Shanghai. Her research interests lie in the general area of signal processing for communications and networking. She currently focuses on localization and communication for underwater wireless sensor networks.

Wenbin Yu (M’18) received the B.Sc. degree in electrical information and automation from Shandong Institute of Architecture and Engineering, Shandong, China, in 2005, the M.Sc. degree in control theory and engineering from Shandong University, Shandong, China, in 2009, and the Ph.D. degree in control science and engineering from Shanghai Jiao Tong University, Shanghai, China, in 2016.

He is currently an Assistant Researcher with the Department of Automation, Shanghai Jiao Tong University. His research interests are in the area of signal processing and information security and privacy for body area networks.

Xinping Guan (M’02–SM’04–F’18) received the B.Sc. degree in mathematics from Harbin Normal University, Harbin, China, in 1986, and the Ph.D. degree in control and systems from the Harbin Institute of Technology, Harbin, China, in 1999.

He is currently a Chair Professor with Shanghai Jiao Tong University, Shanghai, China, where he is also the Deputy Director of the University Research Management Office and the Director of the Key Laboratory of Systems Control and Information Processing, Ministry of Education of China. He has authored and/or coauthored 4 research monographs, more than 270 papers in IEEE Transactions and other peer-reviewed journals, and numerous conference papers. As a Principal Investigator, he has finished/been working on many national key projects. He is the leader of the prestigious Innovative Research Team of the National Natural Science Foundation of China. His current research interests include industrial cyber-physical systems, wireless networking and applications in smart city and smart factory, and underwater sensor networks.

Dr. Guan is an Executive Committee Member of Chinese Automation Association Council and the Chinese Artificial Intelligence Association Council. He was the recipient of the First Prize of Natural Science Award from the Ministry of Education of China in 2006 and 2016, and the Second Prize of the National Natural Science Award of China in 2008. He was also a recipient of the “IEEE TRANSACTIONS ON FUZZY SYSTEMS Outstanding Paper Award” in 2008. He is a “National Outstanding Youth” honored by NSF of China, “Changjiang Scholar” by the Ministry of Education of China, and “State-level Scholar” of “New Century Bai Qianwan Talent Program” of China.